Predictability of Marine Heatwaves off Western Australia using a Linear Inverse Model

Yuxin Wang,[a,b] Neil J. Holbrook,[a,b] and Jules B. Kajtar[a,b,c]

[a] *Institute for Marine and Antarctic Studies, University of Tasmania, Hobart, TAS, Australia*

[b] *Australian Research Council Centre of Excellence for Climate Extremes, University of Tasmania, Hobart, TAS, Australia*

[c] *National Oceanography Centre, Southampton, United Kingdom*

Corresponding author: Yuxin Wang, yuxin.wang@utas.edu.au

Early Online Release: This preliminary version has been accepted for publication in *Journal of Climate*, may be fully cited, and has been assigned DOI 10.1175/JCLI-D-22-0692.1. The final typeset copyedited article will replace the EOR at the above DOI when it is published.

ABSTRACT

Marine heatwaves (MHWs) off Western Australia (110°E−116°E, 22°S−32°S; hereafter, WA MHWs) can cause devastating ecological impacts, as was evidenced by the 2011 extreme event. Previous studies suggest that La Niña is the major large-scale driver of WA MHWs, while Indian Ocean Dipole (IOD) may also play a role. Here, we investigate historical WA MHWs and their connections to these large-scale climate modes in an ocean model (ACCESS−OM2) simulation driven by a prescribed atmosphere from JRA55−do over 1959–2018. Rather than analysing sea surface temperature, the WA MHWs and climate mode indices were characterized and investigated in vertically averaged temperature (VAT) to ~300m depth to afford the longer ocean dynamic time scales, including remote oceanic connections. We develop a cyclostationary linear inverse model (CS-LIM; from 35°S−10°N, across the Indo-Pacific Ocean), to investigate the relative contributions of La Niña VAT and positive IOD VAT to the predictability of WA VAT MHWs. Using a large ensemble of CS-LIM simulations, we found that ~50% of WA MHWs were preceded about 5 months by La Niña, and 30% of the MHWs by positive IOD about 20 months prior. While precursor La Niña or positive IOD, on their own, were found to correspond with increased WA MHW likelihood in the months following (~2.7 times or ~1.5 times more likely than by chance, respectively), in combination these climate mode phases were found to produce the largest enhancement in MHW likelihood (~3.2 times more likely than by chance). Additionally, we found that stronger and longer La Niña and/or positive IOD tend to lead stronger and longer WA MHWs.

Accepted for publication in *Journal of Climate*. DOI 10.1175/JCLI-D-22-0692.1.

SIGNIFICANCE STATEMENT

This study examines seasonal to interannual timescale predictability of marine heatwaves off Western Australia. We developed and applied a linear inverse model, informed by numerical model results, to generate a large number of 60-year temperature simulations across the broader Indian-Pacific Ocean region to quantify this marine heatwave predictability. We found that La Niña typically increases the likelihood of marine heatwaves off Western Australia about 5 months (3-7 months) later, while positive Indian Ocean Dipole events increase their likelihood about 20 months (18-22 months) later. Marine heatwaves can severely impact local marine ecosystems and the economy. Our findings are expected to be valuable for marine heatwave prediction system development on time scales that can be beneficial to marine ecosystem conservation and fishery management.

Accepted for publication in *Journal of Climate*. DOI 10.1175/JCLI-D-22-0692.1.

1. Introduction

In austral late summer to early autumn of 2011, an extreme marine heatwave (MHW) occurred off the coast of Western Australia (WA; Pearce et al. 2011; Hobday et al. 2018). This unprecedented MHW caused extensive marine ecosystem impacts along the WA coast and shelf, including coral bleaching (Depczynski et al. 2013; Wernberg et al. 2013), fish mortality (Pearce & Feng 2013), die-back in seagrass extent (Thomson et al. 2015; Arias-Ortiz et al. 2018), and substantial range decrease in habitat forming kelp (Smale and Wernberg 2013; Wernberg et al. 2013, 2016). In addition, the MHW resulted in mass mortality of local economically important species, including crabs, scallops and lobsters (Caputi et al. 2019). This not only led to local fishery economic losses (Caputi et al. 2016; Molony et al. 2021) but was expected to take at least several years for stock recovery (Caputi et al. 2019). Specifically, stocks of crab and scallop showed recovery ~3-6 years following the 2011 WA MHW while lobster stocks had shown no signs of recovery by 2019 (Caputi et al. 2019). Besides marine ecosystem and economic losses, other studies indicate that austral summer WA MHWs have increased precipitation anomalies over the northwest of Australia, leading to agriculture and water management damages (Tozuka et al. 2014; Doi et al. 2015).

Actions and adaptation responses to help reduce and/or minimize the devastating impacts caused by MHWs may benefit from skillful MHW predictions (Holbrook et al. 2020). To develop effective MHW predictive models, a better understanding of regional MHW predictability and relevant MHW drivers is critical (Holbrook et al. 2019, 2020). While knowledge of the physical processes that give rise to WA MHWs is emerging (e.g., Feng et al. 2013; Benthuysen et al. 2014; Marshall et al. 2015; Tozuka et al. 2021), the predictability of WA MHWs is not well understood. Importantly, MHW predictability on seasonal to interannual and even multi-year time scales is likely to be connected in some way to large−scale climate modes (e.g., El Niño−Southern Oscillation; ENSO; Holbrook et al. 2019). Furthermore, most modes of climate variability are themselves predictable to some extent. For example, the lead time for skillful prediction of ENSO is found to be about six months (e.g., Barnston et al. 2012). The Indian Ocean Dipole (IOD) can be effectively forecast about 1-2 seasons in advance (Luo et al. 2007; Shi et al. 2012; Feng et al. 2022). A recent study suggests possible decadal skill in predicting the IOD (Feba et al. 2021). Hence, understanding WA MHW predictability in the context of ENSO and the IOD may be beneficial to the development of forecast systems with relatively long leads.

Accepted for publication in *Journal of Climate*. DOI 10.1175/JCLI-D-22-0692.1.

The negative (or 'cool') phase of ENSO, known as La Niña, has been identified as the primary large-scale driver of WA MHWs, including the unprecedented 2011 WA MHW (Feng et al. 2013; Benthuysen et al. 2014). La Niña is characterized by increased sea level due to warm upper ocean temperature anomalies in the western tropical Pacific Ocean, which are transported westward via the enhanced Indonesian Throughflow (ITF) and then poleward along the WA coast in the intensified Leeuwin Current, increasing the likelihood of WA MHWs (Pearce and Feng, 2013; Benthuysen et al. 2014; Kataoka et al. 2014; Zinke et al. 2014; Feng et al. 2015; Kido et al. 2016). However, other studies have shown that WA MHWs can also develop without La Niña (Marshall et al. 2015; Kataoka et al. 2018). Further, Zhang et al. (2018) showed that the positive IOD may also play an important role in WA region sea surface warming, with positive IOD occurring one season prior to 30% of the sea surface warm extremes. Although WA MHW predictability from La Niña has been explored to some extent, and we might reasonably expect WA MHW likelihood to increase due to La Niña, the potential contribution from the IOD is less clear. Furthermore, although previous studies have explored WA MHW co-occurrences or lagged occurrences with those climate modes, it is unclear how WA MHW likelihoods change with ENSO and IOD as precursors, or the relative time scales of WA MHW potential predictability.

It is worth noting that many previous studies focus on austral summer (DJF) WA MHWs (e.g., Doi et al. 2013; Feng et al. 2013; Benthuysen et al. 2014; Marshall et al. 2015; Kataoka et al. 2014; Kataoka et al. 2017; Guo et al. 2020; Kusunoki et al. 2020), which are often referred to as Ningaloo Niño (e.g., Feng et al. 2013). In the present study, we instead explore the predictability of WA MHWs that occur in any season. Furthermore, rather than sea surface temperature (SST), the WA MHWs and climate mode indices analysed here were characterised and investigated in vertically averaged temperature (VAT) to ~300m depth to take advantage of the longer time scales in remote connections through the upper ocean dynamics that afford multi-month potential predictability.

We pose the overarching question: To what extent do La Niña and positive IOD provide WA MHW predictability? Specifically, this paper endeavors to answer the following questions: (a) Are La Niña or positive IOD common precursors of WA MHWs? (b) What are the predictability time scales and likelihoods of WA MHWs with La Niña, positive IOD, or a combination of the two? (c) What proportion of WA MHWs are preceded by La Niña, positive IOD events or a combination of the two? (d) Do the opposite phases of ENSO (El

Accepted for publication in *Journal of Climate*. DOI 10.1175/JCLI-D-22-0692.1.

Niño) and IOD (negative IOD phase) suppress WA MHW likelihoods? (e) Are WA MHW metrics (e.g., duration and intensity) connected to the properties of La Niña and/or positive IOD events? To address these questions, we develop an empirical–dynamical model – specifically, a linear inverse model (LIM; Penland and Sardeshmukh 1995), here in a cyclostationary configuration that takes account of the importance of seasonal variations (Shin et al. 2021) – and analyze a large ensemble of LIM-simulated histories of Indian−Pacific Ocean temperatures, founded upon a single realization of an atmosphere-reanalysis-driven ocean simulation (ACCESS-OM2; Bi et al. 2013; Kiss et al. 2020). The motivation for using the LIM is that it can reveal the characteristic linearized dynamics and generate a large ensemble simulation (Penland and Matrosova 1994). This is applied to capture the linearized dynamics of WA MHW evolution and MHW predictability based on a relatively large ensemble of LIM statistics.

2. Data and Methods

a. Ocean temperature data

We analyze monthly-averaged temperatures from a 60-year simulation in the Australian Community Climate and Earth System Simulator (ACCESS) Ocean Model (ocean–sea ice) version 2.0 with 0.1° horizontal resolution (ACCESS−OM2−01: Bi et al. 2013; Kiss et al. 2020), provided by the Consortium for Ocean−Sea Ice Modelling in Australia (COSIMA). The provided ACCESS−OM2−01 simulation was forced by prescribed fluxes calculated from bulk formulae using atmospheric variables from the Japanese 55−Year Reanalysis dataset for driving ocean–sea ice models, version 1.3 (JRA55−do v1.3: Tsujino et al. 2018). The eddy-rich ACCESS−OM2−01 model has been found to better simulate MHWs than with coarser resolutions, with the coarser resolutions simulating less intense MHWs (Pilo et al. 2019). However, to reduce complexity associated with nonlinearities in the eddy-resolving solutions, and hence appropriately characterize MHW predictability under the LIM construction, we chose to re-grid these high-resolution outputs at 1° latitude × 1° longitude. In short, we took advantage of the best physically based simulation of MHWs and re-gridded these to undertake the more basic analysis of MHW predictability in the LIM framework.

In the present study, we have analyzed VAT from the ocean surface to 282m model layer depth (accounting for temperatures that characterize the surface mixed-layer and thermocline

Accepted for publication in *Journal of Climate*. DOI 10.1175/JCLI-D-22-0692.1.

depths in the tropics and subtropics) across the tropical and South Indian and Pacific Oceans, extending meridionally from 35°S−10°N, over the 60-year period from 1959−2018. Vertically averaged temperature anomalies (VATa) were obtained by smoothing the VAT with a 3−month running mean, removing the climatological annual cycle (the climatology was calculated with respect to the full period from 1959–2018), and removing the linear trend at each spatial grid point. Our approach here follows previous LIM studies (e.g., Penland and Sardeshmukh 1995; Newman et al. 2011; Aiken et al. 2013; Vimont et al. 2014; Capotondi and Sardeshmukh 2015; Alexander et al. 2018; Xu et al. 2020), in that we smoothed the raw data before removing the annual cycle and linear trend. The reasons for smoothing the raw data first were to eliminate temporal noise in the raw data, minimize the inherent distortion of statistically determined parameters, and ensure the data meet the foremost constraint of the LIM construction – that is, system linearity (Penland and Matrosova 1994; Penland and Sardeshmukh 1995).

The ACCESS-OM2-01 (hereafter ACCESS-OM2, for brevity) VATa were evaluated against observed and reanalysis data over similar depths (see results in Section 3a later). The monthly observational VAT (1993-2018) used in the evaluation is the Multi Observation Global Ocean 3D Temperature provided by Copernicus Marine (CMEMS; Guinehut et al. 2012; Mulet et al. 2012). The monthly reanalysis VAT used in the evaluation is from the European Centre for Medium-Range Weather Forecasts (ECMWF) ORAS4 (Mogensen et al. 2012; Balmaseda et al. 2013), available from 1959-2016.

While observational or reanalysis data (e.g., CMEMS and ORAS4) could have equally been used, we opted to analyse ACCESS-OM2 for two reasons: (1) The ACCESS-OM2 simulation is self-consistent, in that surface atmospheric forcings are prescribed and the ACCESS-OM2 ocean responses are fully dynamical. Hence, the ocean dynamics associated with the large-scale atmospheric forcings are expected to be simulated in broad agreement with reanalysis or observations (Su et al., 2021). (2) The observational/reanalysis data may be more realistic in the subsurface ocean in more recent times, as more observations have become available. However, the sparsity of subsurface ocean observations in earlier years means that there is likely to be inconsistency in the representation of VAT between the earlier and later years in the observational/reanalysis data.

Accepted for publication in *Journal of Climate*. DOI 10.1175/JCLI-D-22-0692.1.

The model evaluation is based on a comparative analysis of three key indices: WA VAT, Niño3.4 VAT and Dipole Mode Index (DMI) VAT – as a fundamental assessment of the representation of WA MHWs, ENSO (focused here on La Niña as the primary predictor of increased MHW likelihood), and IOD (focused here on positive IOD as the primary predictor of increased MHW likelihood) respectively. WA VAT was calculated by averaging monthly VATa within the region 110°E−116°E, 22°S−32°S (inset in Fig. 1a), which is the same region selected in other recent WA MHW studies (e.g., Marshall et al. 2015; Ryan et al. 2021), and similar to that chosen by others (e.g., Kataoka et al. 2014). Niño3.4 VAT was computed by averaging VATa within the Niño3.4 region (i.e., tropical central Pacific; 5°N−5°S, 170°W−120°W). DMI VAT represents the subsurface IOD signature, and follows the definition of Saji et al. (1999) as the difference between spatially averaged VATa of the western equatorial Indian Ocean (50°E−70°E, 10°S−10°N) and that of the south−eastern equatorial Indian Ocean (90°E−110°E, 10°S−0°N).

b. Linear Inverse Model

The LIM assumes the relevant dynamics can be represented as a linear system forced by stochastic noise, and written in the form of a linear stochastic differential equation:

$$\frac{d\mathbf{x}}{dt} = \mathbf{L}\mathbf{x} + \xi \tag{1}$$

where **x**(t) is the state of the system, **L** is the dynamical operator matrix describing the dynamical features of the evolution of **x,** ξ is the stochastic forcing (i.e., white noise), and t is time. In this study, **x**(t) specifically identifies the smoothed, de-seasonalized and linearly detrended ACCESS−OM2 tropical and South subtropical Indian and Pacific Oceans (35°S−10°N, 20°E−70°W) VATa from 1959-2018 (see further details on the LIM construction in Appendix A; see also Penland and Sardeshmukh (1995) and Shin et al. (2021)).

Note, we refer here to two LIM types: a traditional stationary LIM (ST-LIM; Penland and Sardeshmukh 1995), that ignores seasonal variations, and a cyclostationary LIM (CS-LIM; Shin et al. 2021), which takes account of the seasonal variations. The key difference between the construction of the CS-LIM and ST-LIM is the different computation for the dynamical

Accepted for publication in *Journal of Climate*. DOI 10.1175/JCLI-D-22-0692.1.

operator **L**. In the CS-LIM, **L** is estimated separately for each calendar month (i.e., **L** is seasonally varying), while **L** in the ST-LIM is the same for each calendar month. In our analysis, we found that there is variability in the Niño3.4 and DMI VAT across the annual cycle (a phase-locking of ENSO and the IOD with the seasonal cycle; see discussion for Fig. 2a-c later) – noting that the de-seasonalized anomalies analyzed in this study retain the timing of the existing seasonal phase dependency. Importantly, we found the CS-LIM captures the apparent and important seasonally phase locked co-dependencies, that is ignored in the ST-LIM. The CS-LIM more realistically simulates the seasonal timing of onset and peak of ENSO and IOD events than the ST-LIM. We cannot infer *a priori* that the lead times between ENSO (IOD) events and WA MHWs are going to be more realistic, but the seasonal phase locking natures of ENSO and IOD are nevertheless key and well-represented features, providing confidence in the model representation of the predictors and their timing. Therefore, we chose the CS-LIM configuration for this study.

The LIM is an empirical–dynamical model able to generate climate realizations by numerically integrating the LIM equation (Equation 1) forward in time (Penland and Matrosova 1994). The climate simulations are forced by white noise with observationally constrained spatial structure. In this way, we generated a 120,000-year-long CS-LIM VATa simulation and divided it into a 2000-member 60−year simulation ensemble for analysis (see details in Appendix B), matching the duration of the ACCESS-OM2 simulation. Each ensemble member can be viewed as an alternate realization of the 1959−2018 Indo−Pacific Ocean VATa. Although the CS-LIM simulation ensemble represents a substantial simplification of a large ensemble from coupled climate models, it is vastly computationally cheaper to generate, and may be used to reproduce the large-scale common characteristics of the climate phenomena of interest and their potential dependence on a limited available sample size (Xu et al. 2020). We also examined the sensitivity of the results to the number of simulations. To do this, we randomly chose 1800 simulations of the 2000-member CS-LIM simulation ensemble (90% of the simulation ensemble) 10 times and repeated the analysis. The conclusions drawn in Section 4 and the statistics in Section 5 were found to be insensitive to this reduction in simulation number. Specifically, the evolutions shown in Section 4 did not significantly change and the conclusions derived from statistics of Section 5 were unchanged. These tests suggest that 2000 CS−LIM simulations were a sufficient number for this study.

Accepted for publication in *Journal of Climate*. DOI 10.1175/JCLI-D-22-0692.1.

c. Defining marine heatwaves, La Niña, and positive Indian Ocean Dipole

MHWs are discrete, prolonged, anomalously warm water events, often defined by daily SST exceedances of the 90th percentile threshold, for at least 5 consecutive days, following the definition of Hobday et al. (2016). Here, however, we use a MHW definition to detect MHWs in monthly VAT, rather than daily SST, and so we consider the longer timescale as not only simpler but also more suitable for this vertically integrated analysis of the upper ~300 m, where ocean dynamics are important.

The key reasons we use monthly VAT to detect and analyze WA MHWs in this study are as follows: (1) Monthly data and analyses are appropriate to the longer timescales in the ocean, compared with the atmosphere. Recent studies by Jacox et al. (2020) and Xu et al. (2021) have usefully analyzed monthly data for MHW detection. (2) Monthly observational datasets tend to be longer than those available on daily time scales, providing greater utility for long record analyses. (3) A third significant reason for using VAT rather than SST is that we focus on the potential for longer lead time predictability afforded by the subsurface ocean dynamics (e.g., Holbrook et al. 2020; Lou et al. 2020). While using VAT does not avoid all the effects of local shorter timescale atmospheric influences (e.g., Ekman pumping from local wind stress curl), it would be expected to provide a more complete integration of the upper ocean dynamics from remote influences (e.g. the effects of coastal Kelvin waves and large-scale ocean advection) than SST alone. However, we acknowledge there are some caveats to using VAT: (1) The VAT analysis may not capture all MHWs observed in SST data, since atmospherically driven MHWs tend to warm the water column to lesser depths (Elzahaby et al. 2021), but those driven by ocean advection also tend to be longer-lived (Holbrook et al. 2019, 2020). (2) The VAT analysis might not fully capture the effect of mixed layer depth variations on sea surface warming caused by changes in heat capacity or entrainment (Graham et al. 2014, Tanizaki et al. 2017, and Kataoka et al. 2017), since the VAT provides an average temperature from the ocean's surface down to a depth of 300m and may not reveal a clear signal of the mixed layer depth variation's impact on sea surface warming.

WA MHWs have been characterized here as WA VAT exceedances of the seasonally varying one standard deviation level (1σ) and persisting for at least 3 months. Hence, under this definition, WA MHWs are equally likely throughout all months of the year (Fig. S1 in SI),

Accepted for publication in *Journal of Climate*. DOI 10.1175/JCLI-D-22-0692.1.

unlike in other studies where Ningaloo Niño events have been analyzed as MHW occurrences in the region during the austral summer months of December to February.

La Niña (or El Niño) is defined by the Niño3.4 VAT being less (greater) than minus (plus) one standard deviation ($\pm 1\sigma$) of Niño3.4 VAT for ≥3 months. Likewise, positive (negative) IOD events are defined based on the DMI VAT, following the $\pm 1\sigma$ −intensity for ≥3−months duration criterion. Note that unlike for the WA MHW detection, the $\pm 1\sigma$ levels for ENSO and IOD events are constants, and do not vary seasonally. The $\pm 1\sigma$ values applied to these event detections in each LIM realization are the same, and they were calculated from all LIM realizations.

This study is based solely on VAT, and subsequent references to WA MHWs, La Niña and positive IOD follow this vertically averaged temperature definition, rather than the more common SST definitions. Hence, the timings of observed La Niña and positive IOD based on SST may not precisely coincide with these VAT analyses. Nevertheless, we refer to such events as La Niña or positive IOD for brevity.

Further, for the purpose of clarity and consistency throughout the paper, we refer to the first month of WA MHWs (i.e., the month that WA VAT first exceeds 1σ and persists for ≥3 months) as the "WA MHW onset". Similarly, we use the same terminology for ENSO and IOD events.

3. Model Evaluations

a. ACCESS−OM2

Before analyzing the WA MHWs in ACCESS-OM2, we first evaluated the ACCESS-OM2 simulation as described in Section 2a. We evaluated the WA VAT, Niño3.4 VAT and DMI VAT from ACCESS-OM2 against corresponding VATa calculated from the CMEMS and ORAS4 observational and reanalysis datasets, respectively (Fig. 1).

Accepted for publication in *Journal of Climate*. DOI 10.1175/JCLI-D-22-0692.1.

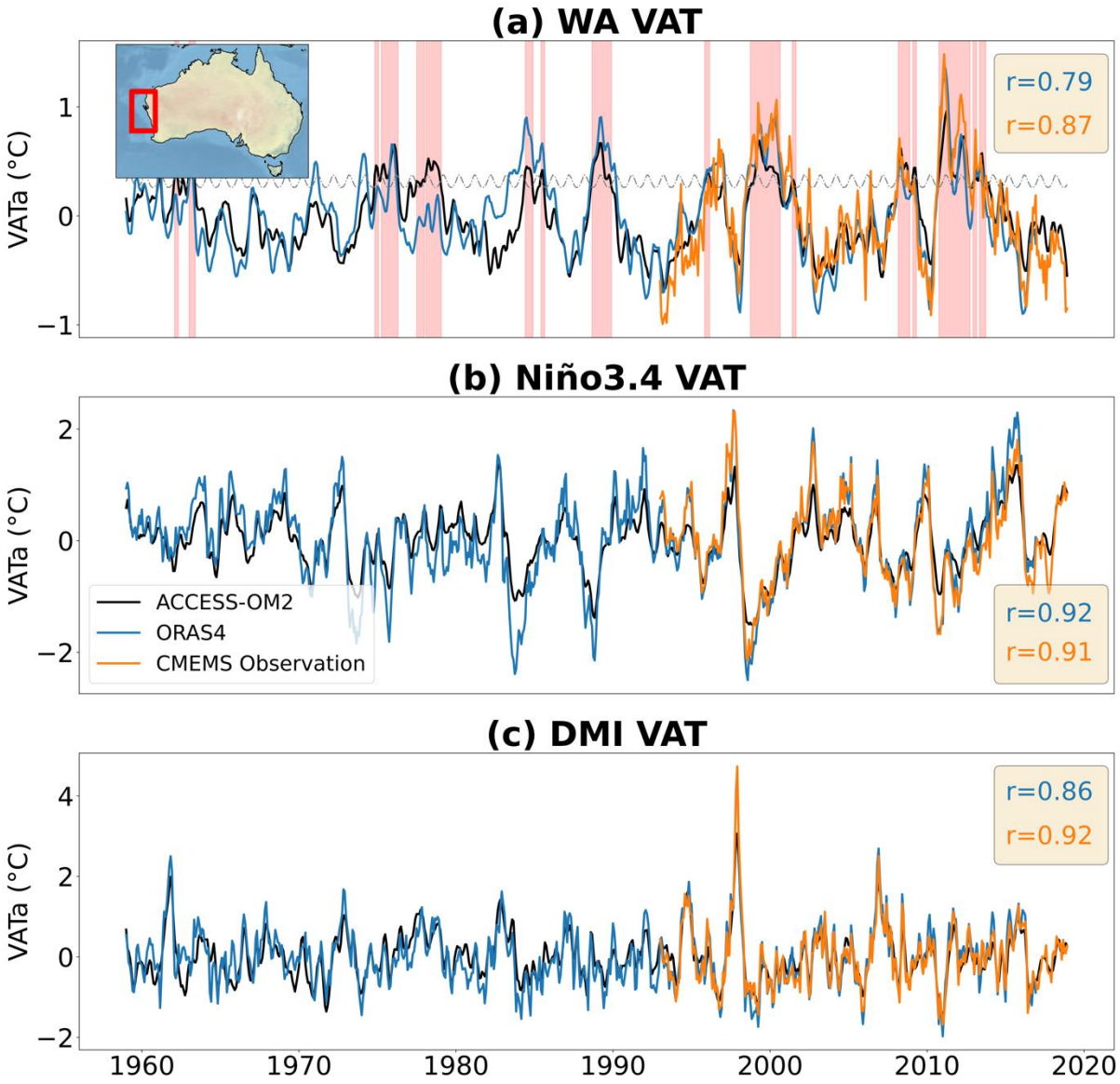

Fig. 1. VAT indices from ACCESS-OM2 over the period 1959-2018, from ORAS4 over 1959-2016, and from CMEMS observational data over 1993-2018. Comparisons and correlations are for **(a)** WA VAT, **(b)** Niño3.4 VAT, and **(c)** DMI VAT. Red vertical bars in **(a)** mark WA MHWs detected by WA VAT from ACCESS-OM2 and the grey dashed line marks the seasonally varying WA MHW intensity threshold. Correlation coefficients between ACCESS-OM2 with ORAS4 and CMEMS observational data for three indices are quoted in blue and orange respectively. Correlations are statistically significant at the 99% level.

The temporal variations in the three indices from all three datasets agree very well, as demonstrated by the strong and statistically significant correlations at the 99% confidence level. We note, however, that ACCESS-OM2 tends to under-represent the extremes seen in the CMEMS observations and ORAS4 reanalysis (i.e., the indices from ACCESS-OM2 have

Accepted for publication in *Journal of Climate*. DOI 10.1175/JCLI-D-22-0692.1.

lower variance). For example, the 1984/85 strong VAT La Niña seen in ORAS4 was not simulated to the same extent in ACCESS-OM2. Although the extremes in ACCESS-OM2 are weaker than in the observations, the strong correlations and hence agreement in the timing of the extreme events supports ACCESS-OM2 as being useful for our study. The under-representation of extremes is somewhat further accounted for by utilizing self-consistent thresholds.

b. CS-LIM Ensemble

Here, we evaluate how well the CS-LIM ensemble reproduces the main features of the ACCESS-OM2 VATa, in comparison to the simpler non-seasonal ST-LIM, as represented in the three indices of primary interest – WA VAT, Niño3.4 VAT, and DMI VAT. The monthly standard deviations, autocorrelations, and power spectral densities of these three indices are shown in Fig. 2.

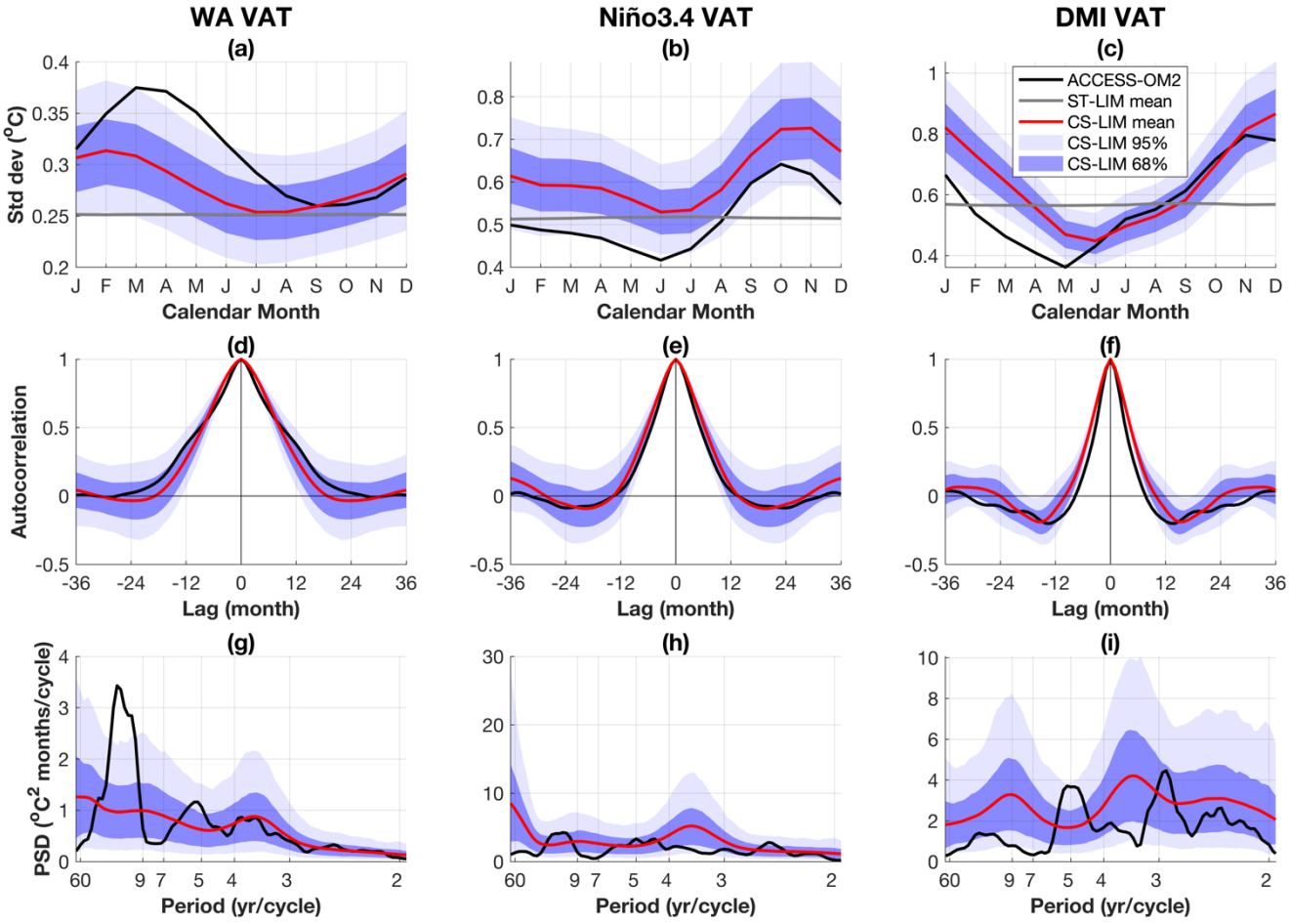

Fig. 2 Comparison between the ACCESS-OM2, ST-LIM and CS-LIM simulations for **(a,d,g)** WA VAT, **(b,e,h)** Niño3.4 VAT and **(c,f,i)** DMI VAT. Shown are the monthly standard

Accepted for publication in *Journal of Climate*. DOI 10.1175/JCLI-D-22-0692.1.

deviation (top row), autocorrelation (middle row) and power spectral density (bottom row) for the three indices. Ensemble spreads are indicated by the 1σ (66%) and 2σ (95%) shaded areas.

The apparent seasonal phase locking of the VAT for WA, Niño3.4, and DMI is evident in each of the monthly standard deviations for ACCESS−OM2 (Fig. 2a-c), with the largest variability occurring in austral autumn, spring, and late spring, respectively, while the smallest variability is in austral spring, winter, and late autumn, respectively. Overall, the CS-LIM was found to reproduce well the seasonal variability as demonstrated by the timing correspondences in the three indices (Fig. 2a-c). However, the standard deviation for the ST−LIM (Fig. 2a-c) is near-constant over all calendar months (by construction). This agrees with Shin et al. (2021), with our CS-LIM capturing the importance of the seasonal variations, whereas the traditional ST-LIM does not. While the monthly standard deviations in the CS-LIM realizations reproduce the seasonal variations of those from ACCESS-OM2, there are some differences in the magnitudes. The variability of WA VAT is weaker in the CS-LIM during the first half of the year, whereas it is stronger overall in Niño3.4 VAT. This is largely due to the CS-LIM realizations having been constructed in a truncated EOF space, with over-representation of ENSO variability and under-representation of WA variability in the leading modes.

For the autocorrelations (Fig. 2d-f), the CS-LIM mimics the features of those from ACCESS-OM2 very well. The ACCESS-OM2 power spectral density falls within the one standard deviation range of the CS-LIM ensemble for most time scales and indices (Fig. 2g-i), but there are some differences. There is a low frequency signal in WA VAT (>10 years) that is not captured in the CS-LIM (Fig. 2g), and the variability of the Niño3.4 VAT is most prominent in the 3- to 4-year band in the CS-LIM (Fig. 2h). Furthermore, the two peaks in the DMI VAT at the 3- and 5-year time scales in ACCESS-OM2 appear to be shifted to longer time scales in the CS-LIM. These differences are not entirely surprising, and they are again likely due to the LIMs being constructed in a truncated EOF space. Further, we find the ACCESS-OM2 power spectrum is noisier than the CS-LIM power spectrum. This is the result of the limited sampling in ACCESS-OM2 (Shin et al. 2021).

4. Western Australia marine heatwave composites

Accepted for publication in *Journal of Climate*. DOI 10.1175/JCLI-D-22-0692.1.

a. Spatial Field Composites

There are 17 discrete WA MHWs in the period 1959−2018 simulated by ACCESS−OM2 (red vertical bars in Fig. 1a), with the most persistent and intense event occurring in 2011. To diagnose the common precursors of WA MHWs, we analyzed the composite spatial evolution of both the ACCESS-OM2 and CS-LIM VATa (in the Indian-Pacific Ocean domain) leading up to the onset of the WA MHWs (Fig. 3).

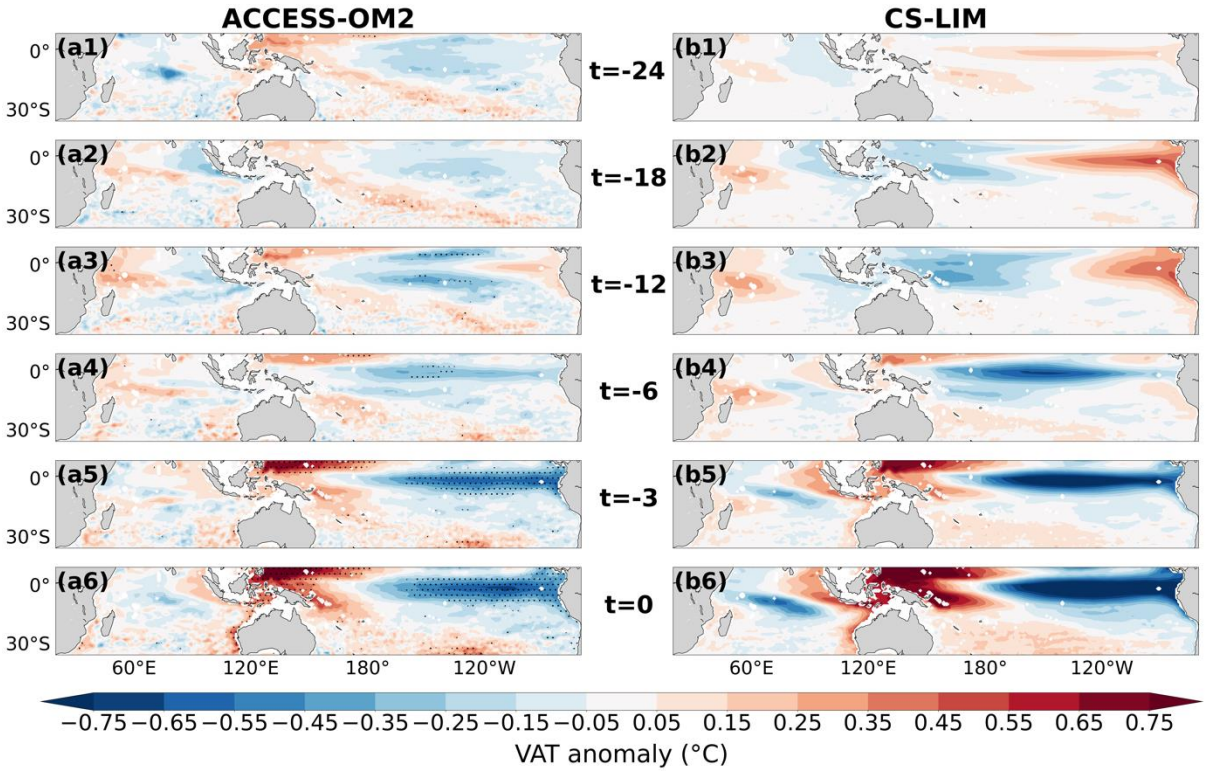

Fig. 3 Composite WA MHW spatial pattern evolutions from ACCESS−OM2 and CS−LIM simulations during the period 1959−2018. (**a1**−**a6**) Composite VATa patterns in ACCESS-OM2 are shown for a range of lead times, from 24 months before WA MHW onset (t=−24 months) to WA MHW onset (t=0 month). (**b1**−**b6**) Same as (**a**) but for VATa composites from the CS−LIM simulations. Stippling in (a) indicates where the ACCESS-OM2 composite VATa is 95% significantly different from zero from a Student's t-test. Due to the large sample size in (b), almost all anomalies are statistically significant at the 95% level, and therefore the stippling is not shown.

Twenty-four months before WA MHW onset in ACCESS-OM2 (Fig. 3(a1)), the Indian Ocean and central-eastern equatorial and South Pacific are generally cooler than normal, while the Maritime Continent and extratropical South Pacific displayed slight warm

Accepted for publication in *Journal of Climate*. DOI 10.1175/JCLI-D-22-0692.1.

anomalies. From t = −18 months (Fig. 3(a2)), the positive IOD pattern (i.e., warmer ocean temperatures in the equatorial western Indian Ocean relative to the east) emerges and persists until t = −12 months (Fig. 3(a3)). From t = −6 months to t = −3 months (Fig. 3(a4)−(a5)), the positive IOD decays but the cold anomalies in the central and eastern equatorial Pacific (i.e., La Niña) develop. The La Niña conditions persist and intensify, and meanwhile the Maritime Continent warm anomalies intensify until the WA MHW onsets at t = 0 months (Fig. 3(a6)). To test the sensitivity of the region chosen for the WA VAT, we repeated this analysis for ACCESS-OM2 using several different WA boxed regions and found the results are relatively insensitive to the choice (not shown).

To test whether La Niña events and/or positive IOD events are common and reliable precursors for WA MHWs from ACCESS-OM2, a Student's t-test was applied to examine if the positive IOD signal from t=−18 months to t=−12 months and La Niña signals from t=−6 months to t=−0 month are significant (i.e., if VATa in the positive IOD and La Niña pattern are statistically significantly different from zero). While La Niña signal shows some significance (black dots in Fig. 3(a4)-(a6)), the positive IOD pattern is less significant.

However, based on only 17 WA MHWs from ACCESS-OM2, the Student's t-test has a caveat - the statistical power values of this t-test are insufficient to be usefully conducted to assess statistical significance due to the small sample size (Fig. S2). Statistical power refers to the probability that the test correctly rejects the null hypothesis, when a specific alternative hypothesis is true (Cohen 1992; Aberson 2015). The statistical power is typically set at 0.8 or higher (Cohen 1992). When the power of a test does not reach 0.8, it could be enhanced by increasing sample size. In this case, a larger sample size is needed for robust conclusions. This motivates the generation of a CS-LIM ensemble, to provide a much larger suite of MHW occurrences than in the single historical record from ACCESS-OM2.

The composite field evolution of all WA MHWs in the CS−LIM ensemble has strong similarities to the composite evolution for ACCESS-OM2 (cf. Fig. 3b and 3a). The positive IOD spatial pattern develops at ~t = –24 months (Fig. 3(b1)) and persists until ~t = –12 months (Fig. 3(b2)–(b3)). La Niña begins to emerge at ~t = –6 months (Fig. 3(b4)) and intensifies before the WA MHW onset (Fig. 3(b5)–(b6)). However, some differences between the composite evolutions of ACCESS−OM2 and CS−LIM exist. For example, the positive IOD pattern lasts longer in the CS-LIM (from ~t = –24 months to ~t = –6 months; Fig. 3(b1)-

Accepted for publication in *Journal of Climate*. DOI 10.1175/JCLI-D-22-0692.1.

(b4)) than in ACCESS-OM2 (Fig. 3a). Nevertheless, the differences are not significant, as the evolution amplitudes from ACCESS−OM2 are within the 95% confidence interval of the CS−LIM ensemble evolution amplitudes almost everywhere.

b. Index Composites

The timing of the co-evolution of the VAT anomalies were further explored in the WA, Niño3.4, and DMI VAT index composites, from 24 months before WA MHW onset and through to 24 months following, in both ACCESS-OM2 and the CS-LIM ensemble (Fig. 4). In ACCESS-OM2 (Fig. 4a), DMI VAT shows that the positive IOD develops at ~t = −20 months and lasts until ~t=-12 months, indicating a tendency for positive IOD to occur >12 months before WA MHW onset. Around the same time, Niño3.4 VAT tends to switch to negative (i.e., La Niña) and peaks at ~t = −2 months, indicating that La Niña events also tend to precede WA MHWs, albeit at a much shorter lead. Again, a Student's t-test was applied (Fig. 4a). However, the t-test power values were insufficient due to the small sample size (Fig. S3), which again highlights the motivation to undertake the CS-LIM simulations.

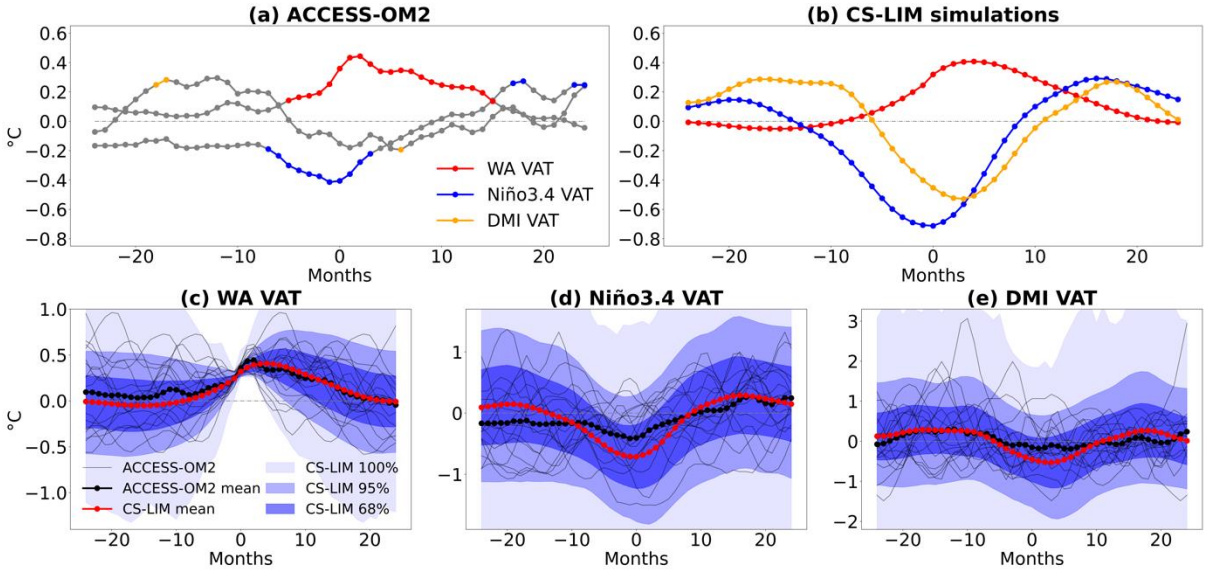

Fig. 4 Time evolution of VAT indices leading up to and following the WA MHWs. (**a**) Composite evolution of WA, Niño3.4, and DMI VAT from 24 months before to 24 months after WA MHW onset in ACCESS-OM2. The grey dots in **(a)** indicate where the ACCESS-OM2 index composite magnitude is not significantly different from zero at the 95% significance level based on a Student's t-test. (**b**) Same as (**a**) but from the CS−LIM simulations. (**c**) WA VAT evolution, aligned with WA MHW onset from ACCESS-OM2 and the CS−LIM simulations. The shaded blue regions indicate the spread of the central 68% and

Accepted for publication in *Journal of Climate*. DOI 10.1175/JCLI-D-22-0692.1.

95% and 100% of the CS-LIM individual realization ensemble. (**d**) and (**e**) are the equivalent figures as (**c**) but for Niño3.4 and DMI VAT respectively.

For the CS-LIM ensemble (Fig. 4b), the positive IOD signal also exists from about t = −20 months, and La Niña evolves no later than ~t = −5 months. This suggests that positive IOD and La Niña conditions do not precede WA MHWs by chance but are indeed common features leading up to WA MHWs. However, it is again evident in this time series composite that the positive IOD peak is flatter and persists longer in the CS-LIM ensemble (from ~t = –24 months to t = –12 months; Fig. 3b) than in ACCESS-OM2 (Fig. 4a).

While the WA MHW evolution in the CS−LIM ensemble composite is similar to that in ACCESS−OM2, some individual WA MHWs in ACCESS−OM2 may be too extreme to be captured by the simplified stochastically forced linear model. To explore this, index evolutions in the CS−LIM simulations and for each individual WA MHW in ACCESS−OM2 were examined (Fig. 4c-e). For WA VAT, most individual ACCESS−OM2 WA MHWs are within the 95% range simulated in the CS−LIM ensemble (Fig. 4c), with only the extreme intensity 2011 WA MHW not completely captured. The CS−LIM ensemble performs well in representing the amplitude of Niño3.4 VAT (Fig. 4d), since the individual ACCESS-OM2 events are within the CS-LIM range. For DMI VAT, two extreme-intensity positive IOD events in ACCESS-OM2 are not fully captured by the CS-LIM range (Fig. 4e).

Overall, we draw two conclusions here: (1) Our CS−LIM simulations capture well the VAT evolutions of WA MHWs in ACCESS−OM2. (2) From our CS-LIM ensemble, we find that positive IOD events and La Niña are indeed common precursors to WA MHWs, which highlights the potential predictability of WA MHWs that may be afforded from tracking these large-scale climate modes. La Niña is found to be a useful predictor about 5 months in advance of WA MHW onset, while positive IOD provides much longer lead time (~20 months) potential predictability for WA MHWs. The results in this section were equivalently regenerated by the ST-LIM. While positive IOD and La Niña signals can be found in the composite evolution of WA MHWs from the ST-LIM simulations (see Fig. S4, S5), the timing of the onset of the two climate modes (especially positive IOD) prior to the WA MHWs does not correspond with the CS-LIM simulations. In the ST-LIM, the positive IOD onset of <18 months prior to WA MHWs represents a shorter lead than the CS-LIM which is

Accepted for publication in *Journal of Climate*. DOI 10.1175/JCLI-D-22-0692.1.

~20 months. This again illustrates that the CS-LIM seasonality is critical to the improved representation of the variability and timing.

5. WA MHW predictability from La Niña and/or positive IOD

In this section, we use the CS-LIM ensemble to robustly determine the extent to which La Niña and positive IOD events drive MHWs off WA, taking two different perspectives. In Section 5a, we aim to quantify the likelihood of WA MHW occurrence due to different climate modes. The La Niña and positive IOD events were first detected and aligned by their onset month, and then the proportions followed by WA MHWs were examined. While in Section 5b, we aim to quantify the proportion of WA MHWs corresponding to different precursor climate conditions. It is the WA MHWs that were first detected and aligned by their onset month, and then the proportions preceded by La Niña or positive IOD conditions were examined. To describe these two sets of analysis another way: at first, we compute the likelihood of the detected climate modes leading to WA MHWs, and then secondly, we compute the likelihood of the detected WA MHWs being preceded by the climate modes. Although these two analyses may appear to be the same, the results from one are not necessarily inferred from the other.

a. Likelihood of positive IOD and/or La Niña leading to WA MHWs

To explore the extent to which La Niña and/or positive IOD events enhance the likelihood of WA MHWs, we quantified the proportions of La Niña and/or positive IOD events that are followed by any WA MHW month (Table 1). Firstly, we determined the most typical predictable window of WA MHWs from La Niña and/or positive IOD. To do this, we detected all WA MHWs in the CS-LIM ensemble, determined their onset time, and then detected the onset time (in months) of the nearest prior La Niña and positive IOD events in the CS-LIM ensemble. We found that La Niña and positive IOD most commonly onset at 5 months and 20 months before the onset of WA MHWs respectively (i.e., t = -5 months and t = -20 months respectively; peaks in Fig. 5a, 5b).

Accepted for publication in *Journal of Climate*. DOI 10.1175/JCLI-D-22-0692.1.

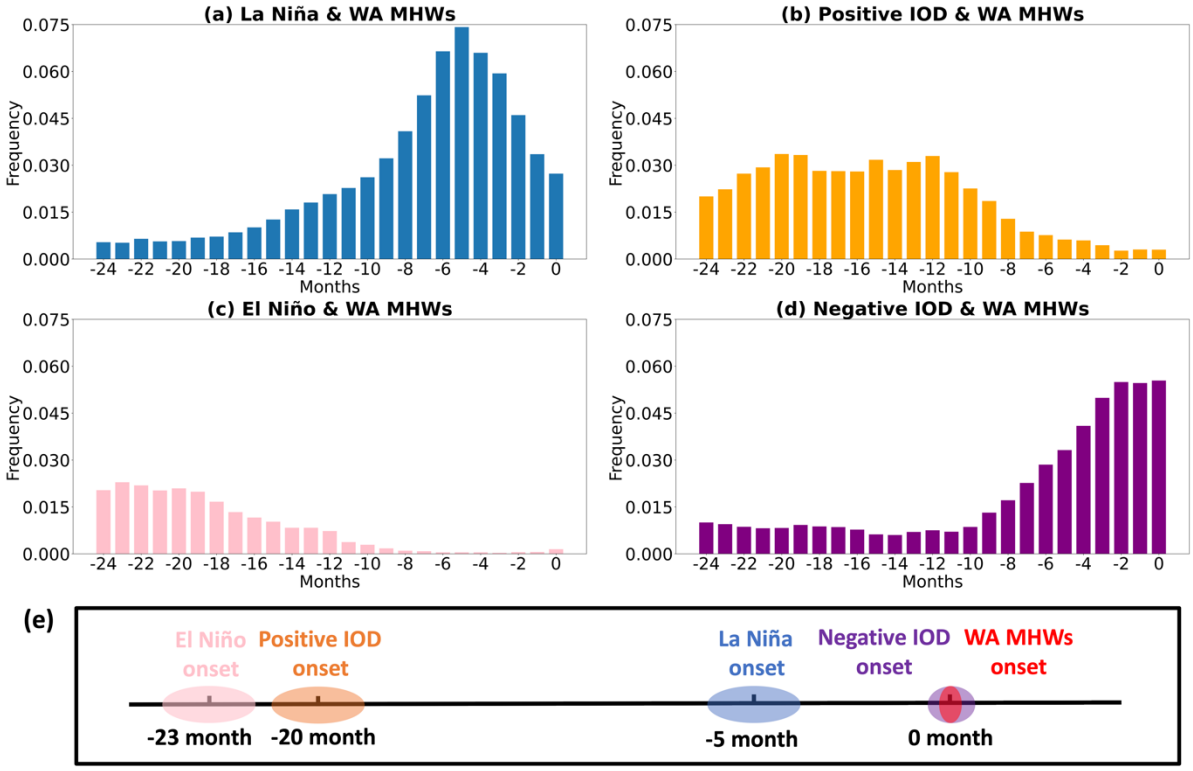

Fig. 5 Onset months of ENSO and IOD events prior to WA MHW onset in the CS-LIM simulations. **(a-d)** Frequency histogram of the onset months of La Niña, positive IOD, El Niño and negative IOD events before WA MHW onset, respectively. t=0 month represents the first month of the WA MHWs. **(e)** Schematic of the most likely time of ENSO/IOD event onsets before WA MHWs.

Besides La Niña and positive IOD, a weak El Niño signal is apparent about 2 years before WA MHW onset, and a negative IOD signal co-occurs with WA MHWs (Fig. 3b, 4b). Positive IOD is sometimes associated with El Niño, which is typically followed by La Niña in the following year (Izumo et al. 2010; Zhang et al. 2021). One may argue that the longer lead time predictability of WA MHWs from positive IOD is because positive IOD is correlated and/or coupled with El Niño and/or La Niña, with either or both being the true precursor of the WA MHWs – that is, the positive IOD may be seen simply as a collinear and possibly coupled process with El Niño and/or La Niña, with El Niño and/or La Niña the 'real drivers' of WA MHWs whereas the positive IOD is an "artificial driver". It might be separately argued that WA MHW predictability from positive IOD is an artefact of WA MHWs being an expression of the negative IOD (i.e., the eastern equatorial Indian Ocean is warmer when the western pole is cooler), with positive IODs tending to flip into the negative IOD phase and thus WA MHWs. Therefore, when examining how La Niña and/or positive

Accepted for publication in *Journal of Climate*. DOI 10.1175/JCLI-D-22-0692.1.

IOD increase the likelihood of WA MHWs, we excluded (or at least minimized) the influence of El Niño and negative IOD. To do this, specifically, we first explored the timing of El Niño and negative IOD occurrences, we found El Niño is most likely to onset at t=-23 months and negative IOD is most likely to onset at t=0 month. Then, when aligning La Niña and/or positive IOD as the precursors of WA MHWs, we excluded the condition when any El Niño and negative IOD occurred at their most typical lead time.

We explored the occurrences of WA MHWs in 5-month windows commencing after the most typical lead time of the climate modes' onset. The choice of MHW window size is arbitrary but selected such that it spanned at least a few months. A range of scenarios was considered:

- "La Niña only": the proportion of La Niña events that are followed by at least one WA MHW month in the 5-month window that commenced 5 months after the onset of La Niña. In other words, the proportion of La Niña events in the CS-LIM ensemble that are followed by a minimum of one WA MHW month during the period of 5-9 months following their onset. Since this is for La Niña only, the 5-month windows preceded by any positive IOD occurrence around its most typical time in the 18-22 months before the WA MHW onset window were excluded from the count. To remove the influence from El Niño and negative IOD, the 5-month windows preceded by any El Niño (negative IOD) occurrence in the months 21-25 months (0-2 months) before the WA MHW onset window were excluded from the count.

- "Positive IOD only": the proportion of positive IOD events that are followed by at least one WA MHW month in the 5-month window that commenced 20 months after the onset of positive IOD. Positive IODs followed by any La Niña occurrence in the 3-7 months before the WA MHW onset window were excluded. Any El Niño (negative IOD) occurrence in the months 21-25 months (0-2 months) before the WA MHW onset window were excluded.

- "Positive IOD and La Niña": the proportion of positive IOD events that are followed by at least one WA MHW month in the 5-month window that commenced 20 months after the onset of positive IOD, but also coinciding with any La Niña occurrence in the 3-7 months before the WA MHW onset window. Any El Niño (negative IOD)

Accepted for publication in *Journal of Climate*. DOI 10.1175/JCLI-D-22-0692.1.

occurrence in the months 21-25 months (0-2 months) before the WA MHW onset window were excluded.

- "El Niño only": the proportion of El Niño events that are followed by at least one WA MHW month in the 5-month window that commenced 23 months after the onset of El Niño. Since this is for El Niño only, the 5-month windows preceded by any positive IOD, La Niña and negative IOD occurrence in the 18-22 months, 3-7 months and 0-2 months respectively before the WA MHW onset window were excluded from the count.

- "Negative IOD only": the proportion of negative IOD events that are followed by at least one WA MHW month in the 5-month window that commenced 0 months after the onset of negative IOD. Since this is for negative IOD only, the 5-month windows preceded by any El Niño, positive IOD and La Niña occurrence in the 21-25 months,18-22 months and 3-7 months respectively before the WA MHW onset window were excluded from the count.

To explore whether the WA MHW likelihood following each condition is changed compared to that under the random chance, we established a reference condition (referred to as the "standard condition"; Table 1) to represent the likelihood of WA MHWs occurring by chance. WA MHW likelihood under the "standard condition" was determined by the proportion of 5-month moving windows (i.e., the same window size as used in the other conditions mentioned above) in the full CS-LIM simulations that contain at least one WA MHW month. Out of all the 5-month moving windows in the CS-LIM simulations, 19.89% of them include at least one WA MHW month, which indicates the random chance of encountering a 5-month window with at least one WA MHW is 19.89%.

Table 1 Proportions of climate modes that are followed by at least one WA MHW month in the 5-month window commencing after the most typical lead time of the climate modes' onset from the CS−LIM simulations. For standard condition, the total number of cases is the count of 5-month moving windows in all CS-LIM simulation months. Since there are 2000×720 simulation months, the count of 5-month moving windows is (2000×720)−4. For other conditions, the total number of cases is the count of each condition across all CS-LIM simulations, whereas the number of cases with MHWs is the count of each condition having at least one MHW month in the 5-month windows commencing after the most typical lead

Accepted for publication in *Journal of Climate*. DOI 10.1175/JCLI-D-22-0692.1.

time of the climate modes' onset. The proportions of cases with MHWs is thus computed from these two numbers.

Conditions	Number of cases		Proportions of cases with MHWs	P-values of chi-square tests with standard condition
	Total	With MHWs		
Standard condition	1,439,996	286,373	19.89%	
La Niña only	10,936	5,873	53.70%	p<0.01
Positive IOD only	14,275	4,283	30.00%	p<0.01
La Niña + positive IOD	2,316	1,460	63.04%	p<0.01
El Niño only	10,803	1,677	15.52%	p<0.01
Negative IOD only	17,297	6,418	37.10%	p<0.01

Under the "La Niña only" condition, for which the influence of positive IOD was not evident, 53.70% of La Niña events are followed by WA MHWs in the appropriate window (Table 1). That is, "La Niña only"-led WA MHWs are ~2.7 times more likely than under the "Standard condition" (or random chance). Under the "Positive IOD only" condition, with no influence from La Niña, there was also an increase in WA MHW likelihood (here, 30.00% compared to 19.89% by chance). But when the positive IOD was also followed by La Niña, we found WA MHW occurrences to increase to 63.04%. Therefore, while La Niña or positive IOD can separately increase the likelihood of WA MHWs, a combination of the two precursor

Accepted for publication in *Journal of Climate*. DOI 10.1175/JCLI-D-22-0692.1.

conditions provides the largest enhancement of WA MHW likelihood. Note that all these three conditions excluded any contribution from El Niño and negative IOD, affirming the roles of positive IOD and La Niña as direct predictors of WA MHWs.

In addition, we examined how El Niño and negative IOD might change WA MHW likelihood. Under the "El Niño only" condition, the proportion of cases with WA MHWs reduced to 15.52%. This indicates the tendency for El Niño to suppress the likelihood of WA MHWs. Under the "Negative IOD" condition, 37.10% of negative IOD events are followed by WA MHWs. However, as negative IOD onset corresponds to the same time as the WA MHW onset (zero-lag), there is limited value from negative IOD in terms of WA MHW seasonal predictability.

To test the robustness of the statistics in Table 1, we performed two tests: (1) We performed chi-square tests based on "Number of cases" column to check whether WA MHW likelihoods following different climate mode phases are statistically significantly different to those under the standard condition. To do this, specifically, we set the null hypothesis as: WA MHW likelihoods following different climate mode phases are not different to those under the standard condition. We found that p-values of all the chi-square tests are all near zero (Table 1), so the null hypothesis can be rejected. This indicates that WA MHW likelihoods under "La Niña only", "positive IOD only", "La Niña and positive IOD" and "negative IOD only" conditions are all statistically significantly higher than under the standard condition (at the >99.99% level). Conversely, WA MHW likelihood under the "El Niño only" condition is significantly lower than that of standard condition (at the >99.99% level). Similarly, we performed another chi-square test on the WA MHW likelihood under the "La Niña and positive IOD" condition, and found that it is statistically significantly higher that under the "La Niña only" condition. In test (2), we reproduced the results by using neighbouring intervals. Specifically, for example, La Niña is most likely to onset at 5 months before WA MHW onset. So, we chose 3-7 months (5-month interval) before WA MHW onset, and then shifted the 5-month interval to 2-6 months (and 4-8 months) to test if the conclusions still hold. Similarly, we shifted the most typical positive IOD interval at 18-22 months to 17-21 months (and 19-23 months) before WA MHW onset. We found that our results were relatively insensitive to slightly shifting the typical intervals, and hence did not affect our conclusions (Table S1).

Accepted for publication in *Journal of Climate*. DOI 10.1175/JCLI-D-22-0692.1.

b. Likelihood of WA MHWs being preceded by La Niña and/or positive IOD

We next used the CS−LIM ensemble to quantify the proportions of WA MHWs that were preceded by La Niña and/or positive IOD. Like the procedure in the previous section, all WA MHWs in the CS-LIM ensemble were first detected, and then those with any La Niña or positive IOD occurrences in specific 5-month windows were tallied. The 5-month window for detecting La Niña was 3-7 months before WA MHW onset, and for positive IOD was 18-22 months prior.

We tested the precursor occurrences under four scenarios, which together sum to 100% (Table 2):

- 'La Niña only': the proportion of WA MHWs with at least one month of La Niña conditions in the 3−7 month window prior to WA MHW onset. Such WA MHW occurrences with any months of positive IOD in the 18-22 month window prior to WA MHW onset were excluded.
- 'Positive IOD only': the proportion of WA MHWs with at least one month of positive IOD conditions in the 18-22 month window prior to WA MHW onset. Such occurrences with any months of La Niña in the 3−7 month window prior to WA MHW onset were excluded.
- 'Both': the proportion of WA MHWs with at least one month of La Niña and at least one month of positive IOD, in the 3−7 month and 18-22 month windows respectively, prior to WA MHW onset.
- 'Neither': the proportion of WA MHWs with neither La Niña nor positive IOD, in the 3−7 month and 18-22 month windows respectively, prior to WA MHW onset.

Table 2 The proportions of WA MHWs corresponding to different precursor climate conditions from the CS−LIM simulations. For "La Niña only", the value indicates the percentage of all WA MHWs in the LIM ensemble preceded by La Niña in a specific timing window, without positive IOD occurrence. It is vice versa for "Positive IOD only".

MHW types	Proportions	
La Niña only	33.14%	La Niña only + Both = 52.08%

Accepted for publication in *Journal of Climate*. DOI 10.1175/JCLI-D-22-0692.1.

Both	18.94%	Positive IOD only + Both = 31.63% La Niña only + Positive IOD only + Both = 64.77%
Positive IOD only	12.69%	
Neither	35.23%	
Total	**100%**	

From the CS-LIM simulations, about 65% of the WA MHWs were preceded by La Niña and/or positive IOD in their respective windows, whilst ~35% of WA MHWs occurred independently (Table 2). This is not to say that those ~35% of WA MHWs were not influenced in some way by either La Niña or positive IOD. They might well have been, to some extent, but the analysis to determine such influences is more complex than the simplified statistical analysis here. Rather, the interesting finding is that ~65% of the WA MHWs correspond with a signature of ENSO or IOD in very specific timing windows. About half of the WA MHWs were preceded by La Niña events (either La Niña only, or in combination with positive IOD), and ~30% were preceded by positive IOD. This suggests that La Niña plays a stronger role than positive IOD in triggering WA MHWs. In addition, we found that ~50% of WA MHWs occurred independently of La Niña (Positive IOD only or Neither; Table 2), or at least without La Niña occurring in that specific timing window, which is in line with previous findings that WA MHWs can develop without La Niña (Marshall et al. 2015; Kataoka et al. 2018). To test the statistical significances of Table 2 values, we randomly chose 1000 members in the 2000-member simulations and reproduced the equivalent table (Table S2). The statistics between Table 2 and Table S2 are not statistically significantly different (at the 95% level) based on a chi-square test. Note that we have examined the statistics in quite narrow time windows, and we recognize that La Niña or positive IOD may play some role in generating or enhancing WA MHWs outside of the selected time frames. Details related to such questions are explored further in the next section.

c. Influence of La Niña and/or positive IOD on WA MHW intensity and duration

To explore whether the properties (e.g., duration and intensity) of La Niña and/or positive IOD may impact WA MHW duration or intensity, we examined the evolution of WA VAT

Accepted for publication in *Journal of Climate*. DOI 10.1175/JCLI-D-22-0692.1.

against the corresponding Niño3.4 and DMI VAT in the CS−LIM ensemble (Fig. 6). Each curve represents the evolution from t = −24 months to t = +12 months binned by WA MHW duration or mean intensity.

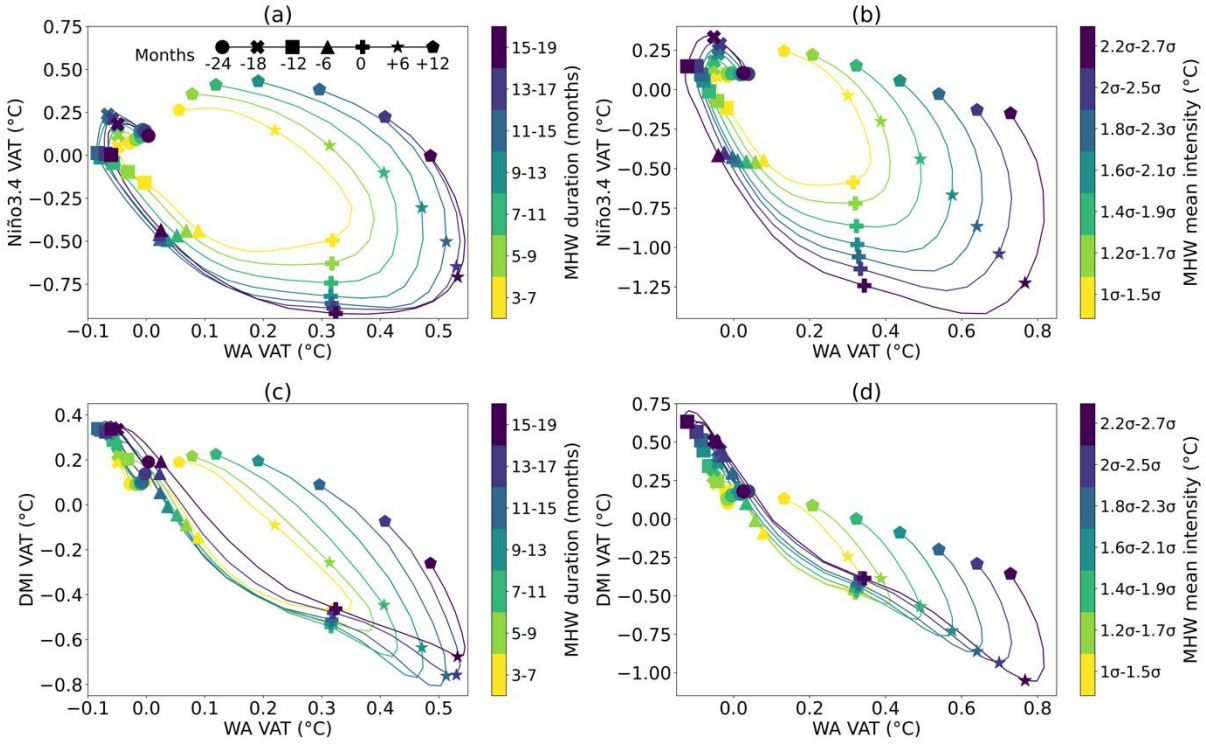

Fig. 6 Evolution of CS−LIM simulated WA MHWs binned by duration and mean intensity, and their relationship to Niño3.4 and DMI VAT. (**a**) Niño3.4 VAT as a function of WA VAT from 24 months prior to WA MHW onset (t=−24 months) to 12 months following (t=+12 months). The curve colour denotes the WA MHW duration, where an overlapping duration interval has been used. Symbols denote a range of timing points in the evolution. (**b**) As in (**a**), but where the WA MHWs are binned by their mean intensity, rather than duration. (**c**,**d**) As in (**a**,**b**), but for DMI VAT rather than Niño3.4 VAT.

As seen in the relationship between Niño3.4 and WA VAT (Fig. 6a, b), La Niña conditions develop, persist, and eventually decay from around t=−6 months (i.e., 6 months before WA MHW onset) to about t=+6 months, in the composite means. It is apparent that longer WA MHWs and more intense WA MHWs are both associated with a stronger negative Niño3.4 VAT (i.e., more intense La Niña) during the period t=−6 months to t=+6 months. This indicates that stronger and longer WA MHWs are assciated with more intense La Niña. In addition, it is clear that more intense La Niñas tend to be longer-lasting (Fig. 6a, b).

Accepted for publication in *Journal of Climate*. DOI 10.1175/JCLI-D-22-0692.1.

Therefore, stronger and longer WA MHWs tend to be associated with stronger and longer duration La Niña.

In the relationship between DMI VAT and WA VAT (Fig. 6c, d), positive IOD can be seen to peak between t=−18 and t=−12 months when binning by WA MHW duration (Fig. 6c), and ~t=−12 months when binning by MHW intensity (Fig. 6d). There is an apparent relationship between the duration of the positive IOD and the WA MHW intensity and duration. This is most clearly seen by comparing DMI VAT values at t=−12 and t=−6 (Fig. 6c). The DMI VAT is a similar magitude for each composite at t=−12, whereas it decreases at t=-6 for shorter duration WA MHWs. Hence, this indicates a tendency for longer positive IODs being associated with stonger and longer WA MHWs. In addition, it can be seen that more intense positive IOD (between t=−12 and t=−6) tends to be associated with stronger and longer WA MHWs (Fig. 6d). The t=−12 to t=−6 timescale for the positive IOD is different to that indicated in the previous sections (~t=-20 months), but the analysis here is indicative of the peak phase of the positive IOD, as oppose to the onset time.

6. Summary and Discussion

Our study has investigated the predictability of Western Australia (WA) marine heatwaves (MHWs) when La Niña and/or positive Indian Ocean Dipole (IOD) events are precursors (or predictors). By constructing a cyclostationary linear inverse model (CS-LIM) – utilizing output from a forced ACCESS-OM2 eddy-rich ocean simulation over the 60-year period from 1959-2018 – we were able to generate large ensembles of simulated vertically averaged temperature (VAT) anomalies (VATa) from 0-282m depth across the tropical and South Indian and Pacific Ocean regions (10^{o}N-35^{o}S), that has improved our undestanding of WA MHW predictability and lead timescales due to these relevant large-scale modes of climate variability.

The evolution of the WA MHWs using the large ensemble CS-LIM simulations confirms that La Niña and positive IOD are indeed important precursors of potential onset for WA MHWs, with La Niña typically preceding WA MHW onset by about 5 months (3-7 months) and positive IOD events tending to occur about 20 months (18-22 months) prior to WA MHW onset. We quantified the proportions of WA MHWs preceded by La Niña, positive IOD, or

Accepted for publication in *Journal of Climate*. DOI 10.1175/JCLI-D-22-0692.1.

their combined influence in the CS-LIM simulations. Although La Niña was confirmed to be the dominant climate precursor, leading to more than half of the WA MHWs simulated, we found that positive IOD provides longer lead time predictability, since it precedes more than 30% of WA MHWs. The increased WA MHW likelihood from the contribution of La Niña, positive IOD events, and in combination, was quantified (a schematic is shown in Fig. 7). We found that both large-scale climatic mode phases can separately increase WA MHW likelihood; WA MHWs were found to be a factor of 2.7 times more likely when only La Niña leads, and a factor of 1.5 times more likely when only positive IOD leads. However, when these mode phases act as precursors in combination, they were found to further increase WA MHW likelihood – specifically, to ~3.2 times more likely compared with random chance. Furthermore, we found that El Niño tends to suppress WA MHW likelihood to only about half the likelihood of random chance. While negative IOD were found to increase WA MHW likelihood, negative onset is about the same time as the WA MHWs (zero-lag), there is limited value from negative IOD in WA MHW seasonal predictability. We also found that stronger and longer La Niña or positive IOD are precursors to stronger and longer WA MHWs. We determined that using a LIM including seasonal variations (i.e., the CS-LIM) is important to capture the WA MHW phase locking apparent in the sophisticated ACCESS-OM2 simulation, which is absent in a standard stationary LIM.

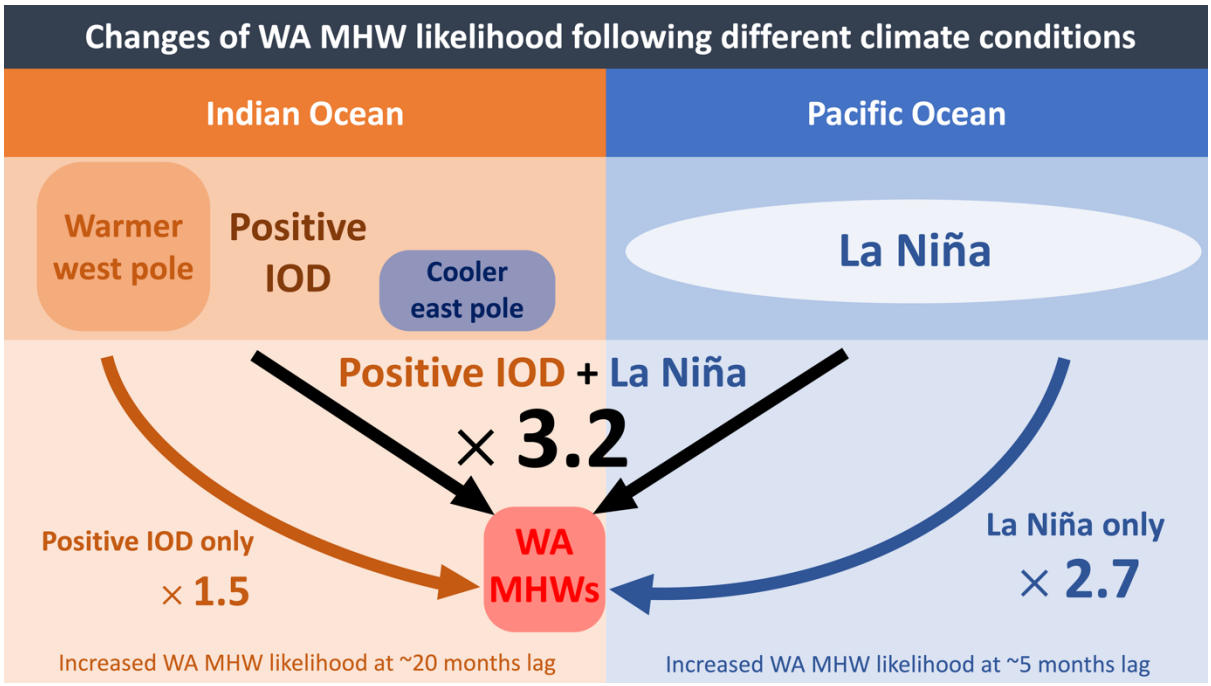

Fig. 7 Schematic of changes of WA MHW likelihood following different climate mode phases (a summary of Table 1 information).

Accepted for publication in *Journal of Climate*. DOI 10.1175/JCLI-D-22-0692.1.

This study has focused on seasonal to interannual timescale predictability of WA MHWs associated with relevant modes of climate variability. Holbrook et al. (2020) highlight that longer lead time (e.g., interannual) predictability of MHWs afforded by climate modes is typically due to their oceanic connections, as the persistence and propagation timescales of oceanic processes are greater than those in the atmosphere. The potential predictability of WA MHWs from La Niña related oceanic processes has been demonstrated in previous studies (e.g., Doi et al. 2013; Feng et al. 2013; Tozuka et al. 2021). In brief, the combined influence of a strengthened southward Leeuwin Current and downwelling Kelvin wave propagation along the WA coast due to La Niña brings more warm water from the equatorial Pacific and Indonesian Throughflow to the WA coast. While longer lead time predictability of WA MHWs from positive IOD has been identified in this study, the key dynamical (or physical) processes that connect positive IOD and enhance WA MHW likelihood remain unclear. We nevertheless expect that this longer lead predictability is most likely due to oceanic processes – in particular, oceanic teleconnections afforded by Rossby/Kelvin wave propagation, for which downwelling waves deepen the thermocline and cause upper ocean warm anomalies. Oceanic Rossby waves take O(months to a year) to propagate westwards across ocean basins in the tropics/subtropics and take O(years to decades) in the midlatitudes, affording multi-month to multi-year potential predictability. Here, in the context of WA MHW predictability time scales, we expect oceanic Rossby/Kelvin waves coupled with upper ocean advection operating between the Indian and Pacific Oceans to be the key sources of these long leads – processes that are currently being further investigated.

The ~20-month lead time WA MHW predictability provided by positive IOD found here seems inconsistent with the finding that positive IOD tends to occur a season before WA coastal sea surface warming (Zhang et al. 2018). Zhang et al. (2018) focused on the WA coast warming at the sea surface, which may be due to atmospheric drivers associated with positive IOD. Indeed, they found that it is the northerly wind anomalies along the WA coast associated with positive IOD that may cause the local sea surface warming. In contrast, in our study focused through the subsurface, via an analysis of VAT to ~300m depth, we are likely to have been able to better capture the the oceanic contributions and connections, affording the longer time scale predictability.

One might argue that using fixed intervals independently determined for ENSO and the IOD may ignore their seasonality in the “La Niña and Positive IOD” condition. We acknowledge

Accepted for publication in *Journal of Climate*. DOI 10.1175/JCLI-D-22-0692.1.

that given ENSO and IOD events have a phase locking nature with the seasonal cycle, pinning the windows to those particular timings is a constraint. But here we were trying to understand the peaks and troughs in the composite plot (and hence it guides our choice of windows), and the two together nevertheless can enhance MHW occurrence. Further, given our definition of WA MHWs relative to a seasonally varying threshold, they can occur year-round, and hence La Niña and positive IOD are truly common precursors for WA MHWs in any season.

The seasonal to interannual timescale predictability of WA MHWs afforded by understanding their relationship with the climate modes explored in this paper may provide some guidance for strategic management decisions in both fisheries and marine conservation. By extension, the development of a prediction system informed by our findings would be potentially beneficial. For example, with lead information of positive IOD and/or La Niña conditions, forecasted higher probabilities of WA MHW event likelihoods may encourage WA fisheries managers to beneficially change target species to those species with high tolerance to warm water (Caputi et al. 2019; Holbrook et al. 2020).

While more than 65% of the WA MHWs investigated in this study were preceded by La Niña and/or positive IOD, the remaining WA MHWs related to neither that may instead be due to shorter-timescale (e.g., subseasonal) processes, including those that are unrelated to large-scale climate modes. The shorter-timescale physical drivers, such as local winds (Kataoka et al. 2014), air-sea heat fluxes (Benthuysen et al. 2014), or the influence of subseasonal-to-seasonal climate variability (e.g., Madden-Julian Oscillation; Marshall et al. 2015; Zhang et al. 2017), can also play important roles. Hence, better understanding these other shorter lead time physical factors is likely to extend the forecast potential over a broader spectrum of WA MHW predictable timescales.

Acknowledgments

We thank the three anonymous reviewers whose suggestions help us to substantially improve this manuscript. The authors thank the Consortium for Ocean-Sea Ice Modelling in Australia (COSIMA; http://www.cosima.org.au) for making the ACCESS-OM2 suite of models available at https://github.com/COSIMA/access-om2. YW would like to thank Jiale Lou, Tongtong Xu and Antonietta Capotondi for conversations about this work. YW

Accepted for publication in *Journal of Climate*. DOI 10.1175/JCLI-D-22-0692.1.

acknowledges support from a PhD scholarship provided by China Scholarship Council (CSC) Grant (202006330005) from the Ministry of Education of the People's Republic of China. YW also acknowledges additional support from a University of Tasmania tuition fee scholarship and Australian Research Council (ARC) Centre of Excellence for Climate Extremes top-up scholarship. NJH and JBK acknowledge support from the ARC Centre of Excellence for Climate Extremes (CE170100023) and the National Environmental Science Program (NESP) Climate Systems Hub. Some of the code used to construct the LIMs in this study was used and adapted from Andre Perkins's stationary LIM python module (https://github.com/frodre/pyLIM). This research was undertaken with the assistance of resources from the National Computational Infrastructure (NCI) supported by the Australian Government.

Data Availability Statement.

The ACCESS-OM2 suite of model simulations are available at https://github.com/COSIMA/access-om2.

APPENDIX A

Linear Inverse Model Construction

As the first step in constructing the linear inverse model (LIM), and consistent with previous studies, an empirical orthogonal function (EOF) analysis was performed on the smoothed, de-seasonalized and linearly detrended ACCESS−OM2 tropical and South Indian and Pacific Oceans (35°S−10°N, 20°E−70°W) vertically averaged temperature anomalies (VATa). We retained the first 12 EOF spatial patterns and corresponding 12 principal components (PCs), which together explained ~69% of the total variance. In this case, **x**(t) in our LIM specifically identifies the first 12 PCs from the EOF analysis for Indo−Pacific Ocean VATa, and **L** is a 12 × 12 dynamical operator matrix.

Typically, in a traditional stationary LIM (i.e., ST-LIM), from Equation 1, the matrix **L** is calculated as:

$$\mathbf{L} = \tau^{-1}\ln[\mathbf{C}(\tau)\mathbf{C}(0)^{-1}], \quad \text{(A1)}$$

Accepted for publication in *Journal of Climate*. DOI 10.1175/JCLI-D-22-0692.1.

where $\mathbf{C}(0)$ is the covariance matrix of vector $\mathbf{x}$ at lag−0, and $\mathbf{C}(\tau) = \langle \mathbf{x}(t+\tau)\mathbf{x}^{T}(t) \rangle$ is the lag-covariance matrix of $\mathbf{x}$ at time lag τ. Substantially, given $\mathbf{L}$, the stochastic forcing ξ in Eq. (1) can be determined from the Lyapunov equation or the fluctuation–dissipation relation (Penland and Matrosova 1994) as:

$$\frac{d\mathbf{C}(0)}{dt} = \mathbf{L}\mathbf{C}(0) + \mathbf{C}(0)\mathbf{L}^{\mathrm{T}} + \mathbf{Q}, \tag{A2}$$

where $\mathbf{Q} = \langle \boldsymbol{\xi}\boldsymbol{\xi}^{T} \rangle dt$ is the covariance matrix of the stochastic forcing multiplied by *dt*.

In the cyclostationary LIM (CS−LIM) used in the present study, the dynamical operator $\mathbf{L}^{\mathrm{CS}}$ varies with calendar months. Two approaches for estimating $\mathbf{L}^{\mathrm{CS}}$ have been suggested by Shin et al. (2021), referred to as "phase-averaged" and "fixed-phase" approaches (OrtizBeviá 1997). We adopted the "fixed-phase" approach here, as the "fixed-phase" approach allows us to use a greater number of EOFs that retain enough SST variance when constructing the LIM (see details in Shin et al. (2021)).

Through application of the "fixed-phase" approach, $\mathbf{L}$ for each month in the CS-LIM can be similarly derived using Equation (A1), but also accounting for seasonal differences, which can be represented by:

$$\mathbf{L}_{\mathrm{j}}^{\mathrm{CS}} = \tau^{-1}\ln\left[\mathbf{C}_{\mathrm{j}}(1)\mathbf{C}_{\mathrm{j}}(0)^{-1}\right], \mathrm{j} = 1,2,3,\ldots,12, \tag{A3}$$

where τ =1 month in our study, and $\mathbf{C}_{\mathrm{j}}(0)$ and $\mathbf{C}_{\mathrm{j}}(1)$ are the covariance matrices of vector $\mathbf{x}_{\mathrm{j}}$ (i.e., $\mathbf{x}$ for calendar month j) at lag−0 and lag−1, respectively. Once $\mathbf{L}_{\mathrm{j}}^{\mathrm{CS}}$ is computed, the stochastic forcing covariance matrix $\mathbf{Q}_{\mathrm{j}}^{\mathrm{CS}}$ in the CS-LIM can be calculated numerically according to Equation (A2):

$$\mathbf{Q}_{\mathrm{j}}^{\mathrm{CS}} = \frac{\mathbf{C}_{\mathrm{j+1}}(0) - \mathbf{C}_{\mathrm{j-1}}(0)}{2\Delta\mathrm{t}} - \mathbf{L}_{\mathrm{j}}^{\mathrm{CS}}\mathbf{C}_{\mathrm{j}}(0) - \mathbf{C}_{\mathrm{j}}(0)(\mathbf{L}_{\mathrm{j}}^{\mathrm{CS}})^{\mathrm{T}}, \mathrm{j} = 1,2,3,\ldots,12, \tag{A4}$$

where $\Delta\mathrm{t} = 1$ month (Shin et al. 2021).

There are at least two conditions that LIMs need to satisfy to ensure they are appropriate and stable. These are: (1) $\mathbf{L}^{\mathrm{CS}}$ must be dissipative. This can be mathematically translated as the magnitudes of the eigenvalues of the monodromy matrix $\mathbf{M} = \mathbf{G}_{\mathrm{T}}^{\mathrm{CS}}\mathbf{G}_{\mathrm{T-1}}^{\mathrm{CS}}\ldots\mathbf{G}_{2}^{\mathrm{CS}}\mathbf{G}_{1}^{\mathrm{CS}}$ are

Accepted for publication in *Journal of Climate*. DOI 10.1175/JCLI-D-22-0692.1.

required to be <1 (T=12 months in this study and $\mathbf{G}_j^{CS} = \exp(\mathbf{L}_j^{CS}), j = 1, 2, 3, \ldots, 12$; See details in Shin et al. (2021)); (2) The stochastic forcing covariance matrices $\mathbf{Q}_j^{CS}$ must be positive definite. However, due to the limited sample sizes available for their estimation, a tolerance is given – it is acceptable for $\mathbf{Q}_j^{CS}$ to have no more than five negative eigenvalues (e.g., Shin et al. 2021). We modified these matrices according to previous LIM research (e.g., Penland 1996; Shin et al. 2021) by setting the negative eigenvalues to zero and then rescaling the positive eigenvalues to maintain the total variance of the stochastic forcing (the trace of $\mathbf{Q}_j^{CS}$).

While we acknowledge that 12 EOFs/PCs is not a very large number of EOFs/PCs retained, this nevertheless explains ~70% of the total variance. Furthermore, 12 is the maximum number of EOFs/PCs we were able to retain and use in order to maintain the CS-LIM stability requirement, comprising of no more than five negative eigenvalues of $\mathbf{Q}_j^{CS}$.

APPENDIX B

Generating LIM simulations

The LIM simulations were carried out following Penland and Matrosova (1994), which represent a two−step integration of the white noise forcing according to:

$$\mathbf{y}(t + \Delta t) = [\mathbf{I} + \mathbf{L}\Delta t]\mathbf{y}(t) + \sqrt{\Delta t}\,\mathbf{S}(t)\mathbf{r}(t), \tag{B1}$$

$$\mathbf{x}\left(t + \frac{\Delta t}{2}\right) = \frac{\mathbf{y}(t + \Delta t) + \mathbf{y}(t)}{2}, \tag{B2}$$

where $\mathbf{S}$ is the stochastic forcing amplitude matrix, which is represented by $\mathbf{S} = \mathbf{\Psi}\mathbf{q}^{\frac{1}{2}}$, where $\mathbf{\Psi}$ and $\mathbf{q}$ are the eigenvectors and corresponding eigenvalues of $\mathbf{Q}$. $\mathbf{\Psi}$, $\mathbf{q}$ and $\mathbf{L}$ are all periodic (period=12) in time for the integration. $\mathbf{r}$ is a random Gaussian white noise vector (i.e., the vector whose mean is 0 and variance is 1).

Accepted for publication in *Journal of Climate*. DOI 10.1175/JCLI-D-22-0692.1.

In this way, we integrated the CS-LIM for 120,060 years from the initial conditions $\mathbf{x}(0) = \mathbf{y}(0) = 0$, with a time step $\Delta t \sim 6$ hours (see Penland and Matrosova (1994) for details). We only used the last 12,000-year CS-LIM simulation, and discarded the first 60-year simulation as the model exercise to remove the initial condition memory. Then we divided the long simulation into a 2000-member 60−year−long Indo−Pacific VATa simulation ensemble for analysis.

REFERENCES

Aberson, C. L., 2015: Statistical Power Analysis. *Emerging Trends in the Social and Behavioral Sciences*, John Wiley & Sons, Ltd, 1–14.

Aiken, C. M., A. Santoso, S. McGregor, and M. H. England, 2013: The 1970's shift in ENSO dynamics: A linear inverse model perspective. *Geophys. Res. Lett.*, **40**, 1612–1617, https://doi.org/https://doi.org/10.1002/grl.50264.

Alexander, M. A., L. Matrosova, C. Penland, J. D. Scott, and P. Chang, 2008: Forecasting Pacific SSTs: Linear inverse model predictions of the PDO. *J. Clim.*, **21**, 385–402, https://doi.org/10.1175/2007JCLI1849.1.

Arias-Ortiz, A., and Coauthors, 2018: A marine heatwave drives massive losses from the world's largest seagrass carbon stocks. *Nat. Clim. Chang.*, **8**, 338–344, https://doi.org/10.1038/s41558-018-0096-y.

Balmaseda, M. A., K. Mogensen, and A. T. Weaver, 2013: Evaluation of the ECMWF ocean reanalysis system ORAS4. *Q. J. R. Meteorol. Soc.*, **139**, 1132–1161, https://doi.org/https://doi.org/10.1002/qj.2063.

Barnston, A. G., M. K. Tippett, M. L. L'Heureux, S. Li, and D. G. DeWitt, 2012: Skill of Real-Time Seasonal ENSO Model Predictions during 2002–11: Is Our Capability Increasing? *Bull. Am. Meteorol. Soc.*, **93**, 631–651, https://doi.org/10.1175/BAMS-D-11-00111.1.

Benthuysen, J., M. Feng, and L. Zhong, 2014: Spatial patterns of warming off Western Australia during the 2011 Ningaloo Niño: Quantifying impacts of remote and local forcing. *Cont. Shelf Res.*, **91**, 232–246, https://doi.org/https://doi.org/10.1016/j.csr.2014.09.014.

Bi, D., and Coauthors, 2013: ACCESS-OM: The ocean and sea-ice core of the ACCESS coupled model. *Aust. Meteorol. Oceanogr. J.*, **63**, 213–232, https://doi.org/10.22499/2.6301.014.

Accepted for publication in *Journal of Climate*. DOI 10.1175/JCLI-D-22-0692.1.

Capotondi, A., and P. D. Sardeshmukh, 2015: Optimal precursors of different types of ENSO events. *Geophys. Res. Lett.*, **42**, 9952–9960, https://doi.org/https://doi.org/10.1002/2015GL066171.

Caputi, N., M. Kangas, A. Chandrapavan, A. Hart, M. Feng, M. Marin, and S. de Lestang, 2019: Factors Affecting the Recovery of Invertebrate Stocks From the 2011 Western Australian Extreme Marine Heatwave. *Front. Mar. Sci.*, **6**, https://doi.org/10.3389/fmars.2019.00484.

Caputi, N., M. Kangas, A. Denham, M. Feng, A. Pearce, Y. Hetzel, and A. Chandrapavan, 2016: Management adaptation of invertebrate fisheries to an extreme marine heat wave event at a global warming hot spot. *Ecol. Evol.*, **6**, 3583–3593, https://doi.org/https://doi.org/10.1002/ece3.2137.

Cohen, J., 1992: A power primer. *Psychological Bulletin*, **112**, 155–159, https://doi.org/10.1037/0033-2909.112.1.155.

Depczynski, M., and Coauthors, 2013: Bleaching, coral mortality and subsequent survivorship on a West Australian fringing reef. *Coral Reefs*, **32**, 233–238, https://doi.org/10.1007/s00338-012-0974-0.

Doi, T., S. K. Behera, and T. Yamagata, 2013: Predictability of the Ningaloo Niño/Niña. *Sci. Rep.*, **3**, 1–7, https://doi.org/10.1038/srep02892.

Doi, T., S. K. Behera, and T. Yamagata, 2015: An interdecadal regime shift in rainfall predictability related to the Ningaloo Niño in the late 1990s. *J. Geophys. Res. Oceans*, **120**, 1388–1396, https://doi.org/10.1002/2014JC010562.

Elzahaby, Y., Schaeffer, A., Roughan, M., and Delaux, S. (2021). Oceanic Circulation Drives the Deepest and Longest Marine Heatwaves in the East Australian Current System. Geophysical Research Letters 48, https://doi/10.1029/2021GL094785.

Feba, F., K. Ashok, M. Collins, and S. R. Shetye, 2021: Emerging Skill in Multi-Year Prediction of the Indian Ocean Dipole. *Front. Clim.*, **3**, https://doi.org/10.3389/fclim.2021.736759.

Feng, M., and Coauthors, 2022: Predictability of sea surface temperature anomalies at the eastern pole of the Indian Ocean Dipole—using a convolutional neural network model. *Front. Clim.*, **4**, https://doi.org/10.3389/fclim.2022.925068.

Feng, M., H. H. Hendon, S.-P. Xie, A. G. Marshall, A. Schiller, Y. Kosaka, N. Caputi, and A. Pearce, 2015: Decadal increase in Ningaloo Niño since the late 1990s. *Geophys. Res. Lett.*, **42**, 104-112, https://doi.org/10.1002/2014GL062509.

Feng, M., M. J. McPhaden, S. P. Xie, and J. Hafner, 2013: La Niña forces unprecedented Leeuwin Current warming in 2011. *Sci. Rep.*, **3**, 1–9, https://doi.org/10.1038/srep01277.

Graham, F. S., J. N. Brown, C. Langlais, S. J. Marsland, A. T. Wittenberg, and N. J. Holbrook, 2014: Effectiveness of the Bjerknes stability index in representing ocean dynamics. *Clim. Dyn.*, **43**, 2399-2414, https://doi.org/10.1007/s00382-014-2062-3.

Accepted for publication in *Journal of Climate*. DOI 10.1175/JCLI-D-22-0692.1.

Guinehut, S., A.-L. Dhomps, G. Larnicol, and P.-Y. Le Traon, 2012: High resolution 3-D temperature and salinity fields derived from in situ and satellite observations. *Ocean Sci.*, **8**, 845–857, https://doi.org/10.5194/os-8-845-2012.

Guo, Y., Y. Li, F. Wang, Y. Wei, and Z. Rong, 2020: Processes Controlling Sea Surface Temperature Variability of Ningaloo Niño. *Journal of Climate*, **33**, 4369–4389, https://doi.org/10.1175/JCLI-D-19-0698.1.

Hobday, A. J., and Coauthors, 2016: A hierarchical approach to defining marine heatwaves. *Prog. Oceanogr.*, **141**, 227–238, https://doi.org/10.1016/j.pocean.2015.12.014.

Hobday, A. J., and Coauthors, 2018: Categorizing and Naming Marine Heatwaves. *Oceanography*, **31**, 162–173.

Holbrook, N. J., and Coauthors, 2019: A global assessment of marine heatwaves and their drivers. *Nat. Commun.*, **10**, 1–13, https://doi.org/10.1038/s41467-019-10206-z.

Holbrook, N. J., A. Sen Gupta, E. C. J. Oliver, A. J. Hobday, J. A. Benthuysen, H. A. Scannell, D. A. Smale, and T. Wernberg, 2020: Keeping pace with marine heatwaves. *Nat. Rev. Earth Environ.*, https://doi.org/10.1038/s43017-020-0068-4.

Izumo, T., and Coauthors, 2010: Influence of the state of the Indian Ocean Dipole on the following year's El Nĩno. *Nat. Geosci.*, **3**, 168–172, https://doi.org/10.1038/ngeo760.

Jacox, M. G., M. A. Alexander, S. J. Bograd, and J. D. Scott, 2020: Thermal displacement by marine heatwaves. *Nature*, **584**, 82–86, https://doi.org/10.1038/s41586-020-2534-z.

Kataoka, T., S. Masson, T. Izumo, T. Tozuka, and T. Yamagata, 2018: Can Ningaloo Niño/Niña Develop Without El Niño–Southern Oscillation? *Geophys. Res. Lett.*, **45**, 7040–7048, https://doi.org/10.1029/2018GL078188.

Kataoka, T., T. Tozuka, S. Behera, and T. Yamagata, 2014: On the Ningaloo Niño/Niña. *Clim. Dyn.*, **43**, 1463–1482, https://doi.org/10.1007/s00382-013-1961-z.

Kataoka, T., T. Tozuka, and T. Yamagata, 2017: Generation and decay mechanisms of Ningaloo Niño/Niña. J. *Geophys. Res. Lett.*, **122**, 8913-8932, https://doi.org/10.1002/2017JC012966.

Kido, S., T. Kataoka, and T. Tozuka, 2016: Ningaloo Niño simulated in the CMIP5 models. *Clim. Dyn*, **47**, 1469-1484, https://doi.org/10.1007/S00382-015-2913-6.

Kiss, A., and Coauthors, 2019: ACCESS-OM2: A Global Ocean-Sea Ice Model at Three Resolutions. *Geosci. Model Dev. Discuss.*, 1–58, https://doi.org/10.5194/gmd-2019-106.

Kusunoki, H., S. Kido, and T. Tozuka, 2020: Contribution of oceanic wave propagation from the tropical Pacific to asymmetry of the Ningaloo Niño/Niña. *Clim. Dyn.*, **54**, 4865–4875, https://doi.org/10.1007/s00382-020-05268-5.

Accepted for publication in *Journal of Climate*. DOI 10.1175/JCLI-D-22-0692.1.

Lou, J., T. J. O'Kane, and N. J. Holbrook, 2020: A Linear Inverse Model of Tropical and South Pacific Seasonal Predictability. *J. Climate*, **33**, 4537–4554, https://doi.org/10.1175/JCLI-D-19-0548.1.

Luo, J.-J., S. Masson, S. Behera, and T. Yamagata, 2007: Experimental Forecasts of the Indian Ocean Dipole Using a Coupled OAGCM. *J. Clim.*, **20**, 2178–2190, https://doi.org/10.1175/JCLI4132.1.

Marshall, A. G., H. H. Hendon, M. Feng, and A. Schiller, 2015: Initiation and amplification of the Ningaloo Niño. *Clim. Dyn.*, **45**, 2367–2385, https://doi.org/10.1007/s00382-015-2477-5.

Mogensen, K., and A. W. M. Alonso Balmaseda, 2012: The NEMOVAR ocean data assimilation system as implemented in the ECMWF ocean analysis for System 4. 59, https://doi.org/10.21957/x5y9yrtm.

Molony, B. W., D. P. Thomson, and M. Feng, 2021: What Can We Learn From the 2010/11 Western Australian Marine Heatwave to Better Understand Risks From the One Forecast in 2020/21? *Front. Mar. Sci.*, **8**, 8–11, https://doi.org/10.3389/fmars.2021.645383.

Mulet, S., M.-H. Rio, A. Mignot, S. Guinehut, and R. Morrow, 2012: A new estimate of the global 3D geostrophic ocean circulation based on satellite data and in-situ measurements. *Deep Sea Res. Part II Top. Stud. Oceanogr.*, **77**–**80**, 70–81, https://doi.org/https://doi.org/10.1016/j.dsr2.2012.04.012.

Newman, M., M. A. Alexander, and J. D. Scott, 2011: An empirical model of tropical ocean dynamics. *Clim. Dyn.*, **37**, 1823, https://doi.org/10.1007/s00382-011-1034-0.

Oliver, E. C. J., and Coauthors, 2019: Projected Marine Heatwaves in the 21st Century and the Potential for Ecological Impact. *Front. Mar. Sci.*, **6**, 734.

OrtizBeviá, M. J., 1997: Estimation of the cyclostationary dependence in geophysical data fields. *J. Geophys. Res. Atmos.*, **102**, 13473–13486, https://doi.org/https://doi.org/10.1029/97JD00243.

Pearce, A., R. Lenanton, G. Jackson, J. Moore, M. Feng, and D. Gaughan, 2011: *The "marine heat wave" off Western Australia during the summer of 2010/11. Fisheries Research Report No. 222. Department of Fisheries, Western Australia*. 40 pp.

Penland, C., 1996: A stochastic model of IndoPacific sea surface temperature anomalies. *Phys. D Nonlinear Phenom.*, **98**, 534–558, https://doi.org/https://doi.org/10.1016/0167-2789(96)00124-8.

Penland, C., and L. Matrosova, 1994: A Balance Condition for Stochastic Numerical Models with Application to the El Niño-Southern Oscillation. *J. Clim.*, **7**, 1352–1372, https://doi.org/10.1175/1520-0442(1994)007<1352:ABCFSN>2.0.CO;2.

Accepted for publication in *Journal of Climate*. DOI 10.1175/JCLI-D-22-0692.1.

Penland, C., and P. D. Sardeshmukh, 1995: The Optimal Growth of Tropical Sea Surface Temperature Anomalies. *J. Clim.*, **8**, 1999–2024, https://doi.org/10.1175/1520-0442(1995)008<1999:TOGOTS>2.0.CO;2.

Pilo, G. S., N. J. Holbrook, A. E. Kiss, and A. M. Hogg, 2019: Sensitivity of Marine Heatwave Metrics to Ocean Model Resolution. *Geophys. Res. Lett.*, **46**, 14604–14612, https://doi.org/https://doi.org/10.1029/2019GL084928.

Ryan, S., C. C. Ummenhofer, G. Gawarkiewicz, P. Wagner, M. Scheinert, A. Biastoch, and C. W. Böning, 2021: Depth Structure of Ningaloo Niño/Niña Events and Associated Drivers. *J. Clim.*, **34**, 1767–1788, https://doi.org/10.1175/JCLI-D-19-1020.1.

Sen Gupta, A., J. A. Benthuysen, M. T. Burrows, M. G. Donat, N. J. Holbrook, P. J. Moore, M. S. Thomsen, and T. Wernberg, 2018: Categorizing and Naming Marine Heatwaves. *Oceanography*, **31**, 162–173.

Shi, L., H. Hendon, O. Alves, J.-J. Luo, M. Balmaseda, and D.L.T.Anderson, 2012: How Predictable is the Indian Ocean Dipole? *Mon. Weather Rev.*, **140**, https://doi.org/10.1175/MWR-D-12-00001.1,.

Shin, S. I., P. D. Sardeshmukh, M. Newman, C. Penland, and M. A. Alexander, 2021: Impact of annual cycle on ENSO variability and predictability. *J. Clim.*, **34**, 171–193, https://doi.org/10.1175/JCLI-D-20-0291.1.

Smale, D. A., and T. Wernberg, 2013: Extreme climatic event drives range contraction of a habitat-forming species. *Proc. R. Soc. B Biol. Sci.*, **280**, https://doi.org/10.1098/rspb.2012.2829.

Tanizaki, C., T. Tozuka, T. Doi, and T. Yamagata, 2017: Relative importance of the processes contributing to the development of SST anomalies in the eastern pole of the Indian Ocean Dipole and its implication for predictability. *Clim Dyn.*, **49**, 1289-1304, doi:10.1007/s00382-016-3382-2.

Thomson, J. A., D. A. Burkholder, M. R. Heithaus, J. W. Fourqurean, M. W. Fraser, J. Statton, and G. A. Kendrick, 2015: Extreme temperatures, foundation species, and abrupt ecosystem change: an example from an iconic seagrass ecosystem. *Glob. Chang. Biol.*, **21**, 1463–1474, https://doi.org/10.1111/gcb.12694.

Tozuka, T., M. Feng, W. Han, S. Kido, and L. Zhang, 2021: 8 - The Ningaloo Niño/Niña: Mechanisms, relation with other climate modes and impacts. S.K.B.T.-T. and E.A.-S.I. Behera, Ed., Elsevier, 207–219.

Tozuka, T., T. Kataoka, and T. Yamagata, 2014: Locally and remotely forced atmospheric circulation anomalies of Ningaloo Niño/Niña. *Clim. Dyn.*, **43**, 2197–2205, https://doi.org/10.1007/s00382-013-2044-x.

Tsujino, H., and Coauthors, 2018: JRA-55 based surface dataset for driving ocean–sea-ice models (JRA55-do). *Ocean Model.*, **130**, 79–139, https://doi.org/10.1016/j.ocemod.2018.07.002.

Accepted for publication in *Journal of Climate*. DOI 10.1175/JCLI-D-22-0692.1.

Vimont, D. J., M. A. Alexander, and M. Newman, 2014: Optimal growth of Central and East Pacific ENSO events. *Geophys. Res. Lett.*, **41**, 4027–4034, https://doi.org/10.1002/2014GL059997.

Wernberg, T., and Coauthors, 2016: Climate-driven regime shift of a temperate marine ecosystem. *Science (80-.).*, **353**, 169–172, https://doi.org/10.1126/science.aad8745.

Wernberg, T., D. A. Smale, F. Tuya, M. S. Thomsen, T. J. Langlois, T. De Bettignies, S. Bennett, and C. S. Rousseaux, 2013: An extreme climatic event alters marine ecosystem structure in a global biodiversity hotspot. *Nat. Clim. Chang.*, **3**, 78–82, https://doi.org/10.1038/nclimate1627.

Xu, T., M. Newman, A. Capotondi, and E. Di Lorenzo, 2021: The Continuum of Northeast Pacific Marine Heatwaves and Their Relationship to the Tropical Pacific. *Geophys. Res. Lett.*, **48**, 1–10, https://doi.org/10.1029/2020GL090661.

Zhang, L., W. Han, Y. Li, and T. Shinoda, 2018: Mechanisms for generation and development of the Ningaloo Niño. *J. Clim.*, **31**, 9239–9259, https://doi.org/10.1175/JCLI-D-18-0175.1.

Zhang, L., W. Han, G. A. Meehl, A. Hu, N. Rosenbloom, T. Shinoda, and M. J. McPhaden, 2021: Diverse impacts of Indian Ocean Dipole on El Niño-Southern Oscillation. *J. Clim.*, 1–46, https://doi.org/10.1175/jcli-d-21-0085.1.

Zhang, N., M. Feng, H. H. Hendon, A. J. Hobday, and J. Zinke, 2017: Opposite polarities of ENSO drive distinct patterns of coral bleaching potentials in the southeast Indian Ocean. *Sci. Rep.*, **7**, 1–10, https://doi.org/10.1038/s41598-017-02688-y.

Zinke, J., A. Rountrey, M. Feng, S. P. Xie, and D. Dissard, 2014: Corals record long-term Leeuwin Current variability including Ningaloo Niño/Niña since 1795. *Nat. Commun.*, **5**, 3607, https://doi.org/10.1038/ncomms4607.

Accepted for publication in *Journal of Climate*. DOI 10.1175/JCLI-D-22-0692.1.